Atmos. Chem. Phys. Discuss., 11, 2873–2929, 2011
www.atmos-chem-phys-discuss.net/11/2873/2011/
doi:10.5194/acpd-11-2873-2011

Atmospheric Chemistry and Physics Discussions

Atmospheric sulfur cycling in the Southeastern Pacific – longitudinal distribution, vertical profile, and diel variability observed during VOCALS-REx

M. Yang[1], B. J. Huebert[1], B. W. Blomquist[1], S. G. Howell[1], L. M. Shank[1], C. S. McNaughton[1], A. D. Clarke[1], L. N. Hawkins[2], L. M. Russell[2], D. S. Covert[3], D. J. Coffman[4], T. S. Bates[4], P. K. Quinn[4], N. Zagorac[5], A. R. Bandy[5], S. P. de Szoeke[6], P. D. Zuidema[7], S. C. Tucker[8], W. A. Brewer[9], K. B. Benedict[10], and J. L. Collett[10]

[1]University of Hawaii at Manoa, Department of Oceanography, Honolulu, HI, USA
[2]University of California San Diego, Scripps Institute of Oceanography, La Jolla, CA, USA
[3]University of Washington, Department of Atmospheric Sciences, Seattle, WA, USA
[4]National Oceanographic and Atmospheric Administration, Pacific Marine Environmental Laboratory, Seattle, WA, USA
[5]Drexel University, Department of Chemistry, Philadelphia, PA, USA
[6]Oregon State University, College of Oceanic and Atmospheric Sciences, Corvallis, OR, USA

[7]University of Miami, Rosenstiel School of Marine and Atmospheric Science, Miami, FL, USA
[8]Ball Aerospace and Technologies, Corp., Boulder, CO, USA
[9]National Oceanographic and Atmospheric Administration, Earth System Research Laboratory, Boulder, CO, USA
[10]Colorado State University, Department of Atmospheric Science, Fort Collins, CO, USA

Received: 10 January 2011 – Accepted: 11 January 2011 – Published: 24 January 2011

Correspondence to: B. J. Huebert (huebert@hawaii.edu)

Published by Copernicus Publications on behalf of the European Geosciences Union.

Abstract

Dimethylsulfide (DMS) emitted from the ocean is a biogenic precursor gas for sulfur dioxide (SO_2) and non-sea-salt sulfate aerosols (SO_4^{2-}). During the VAMOS-Ocean-Cloud-Atmosphere-Land Study Regional Experiment (VOCALS-REx) in 2008, multiple instrumented platforms were deployed in the Southeastern Pacific (SEP) off the coast of Chile and Peru to study the linkage between aerosols and stratocumulus clouds. We present here observations from the NOAA Ship *Ronald H. Brown* and the NSF/NCAR C-130 aircraft along ~20° S from the coast (70° W) to a remote marine region (85° W). While SO_4^{2-} and SO_2 concentrations were distinctly elevated above background levels in the coastal marine boundary layer (MBL) due to anthropogenic influence (~800 and 80 pptv, respectively), their concentrations rapidly decreased offshore (~100and 25 pptv). Compared to the "mass" entrainment fluxes of SO_4^{2-} and SO_2 from the free troposphere (0.5± 0.3 and 0.3± 0.2 μmoles m^{-2} day^{-1}), the sea-to-air DMS flux (3.8± 0.1 μmoles m^{-2} day^{-1}) remained the predominant source of sulfur mass to the MBL. In-cloud oxidation was found to be the most important mechanism for SO_2 removal and in situ SO_4^{2-} production. Surface SO_4^{2-} loading in the remote region displayed pronounced diel variability, increasing rapidly in the first few hours after sunset and then decaying for the rest of the time. We theorize that the increase in SO_4^{2-} was due to nighttime recoupling of the MBL that mixed down cloud-processed air, while decoupling and sporadic precipitation scavenging were responsible for the daytime decline in SO_4^{2-}.

1 Introduction

The ocean is the largest source of natural reduced sulfur gas to the atmosphere, most of which is in the form of dimethylsulfide (DMS), a volatile organic compound produced from phytoplankton. The annual global sea-to-air DMS emission is estimated to be 15 ~ 33 Tg S (Kettle and Andreae, 2000), depending on the gas exchange and wind

ACPD
11, 2873–2929, 2011

speed parameterization. In the atmosphere, DMS is principally oxidized by the hydroxyl radical (OH) to a number of products, including sulfur dioxide (SO_2). In addition to DMS oxidation, SO_2 is formed from fossil fuel combustion and biomass burning and removed from the MBL through deposition to the ocean surface and oxidative reactions in the gas and aqueous phase. Gas phase oxidation of SO_2 by OH and subsequent reactions with water vapor yield sulfuric acid vapor ($H_2SO_{4(g)}$), which usually condenses upon preexisting aerosol surfaces and increases non-sea-salt sulfate aerosol (SO_4^{2-}) mass. Under specific conditions (usually high $H_2SO_{4(g)}$and water vapor as well as low aerosol surface area), $H_2SO_{4(g)}$ may undergo gas-to-particle conversion and nucleate new nm-sized particles, which then grow by condensation and coagulation (Perry et al., 1994; Clarke et al., 1998).

Generally the oxidation of SO_2 in the aqueous phase, which also leads to fine (submicron) SO_4^{2-} aerosols, is much faster than in the gas phase. Due to dissolution of CO_2 and other acids, cloud water typically has a pH under 5 (Chameides, 1984), which makes hydrogen peroxide (H_2O_2) the principal oxidant of SO_2 in cloud. Hegg (1985) suggested cloud processing to be the most important mechanism for the conversion from SO_2 to SO_4^{2-}. Sea-salt aerosols from wave breaking account for the majority of the coarse (supermicron) number as well as total aerosol mass, and tend to be more basic than fine SO_4^{2-} aerosols because of the initial alkalinity of seawater (pH $\sim$ 8.1) and its carbonate buffering capacity. Because the reaction rate between SO_2 and ozone (O_3) is greatly accelerated at high pH (Hoffmann, 1986), some authors postulated O_3 oxidation in sea-salt aerosols to be a significant sink of SO_2 and source of SO_4^{2-} mass (Sievering et al., 1991; Faloona et al., 2010).

In addition to affecting atmospheric chemistry, SO_4^{2-} aerosols are climatically important because they alter the global radiative balance directly by scattering light (Charlson et al., 1992) and indirectly by controlling the optical properties, areal extent, and lifetimes of clouds by acting as cloud condensation nuclei (CCN). In a remote marine environment where CCN represent a large fraction of the aerosol number, a gap at 70 $\sim$ 80 nm in diameter in the number distribution is often observed, which has been

ACPD
11, 2873–2929, 2011

coined the “Hoppel minimum” (Hoppel et al., 1986). Aerosols smaller than this minimum are unactivated and sometimes called Aitken particles, while larger aerosols have been activated and grown through cloud processing into the accumulation mode (0.1 ∼ 1 um).

Charlson et al. (1987) coined the “CLAW” hypothesis, which postulated a negative feedback loop from enhanced phytoplankton growth and DMS efflux in a warming climate to a decrease in incident radiation (and hence cooling) due to greater albedo of marine clouds from more SO_4^{2-} derived CCN. The effects of naturally derived SO_4^{2-} on clouds are expected to be greatest in areas deprived of CCN (Twomey, 1991), such as over the remote ocean in the relatively pristine Southern Hemisphere.

The Southeastern Pacific (SEP) is a region characterized by large-scale subsidence associated with subtropical anticyclonic flow, coastal upwelling of cold water driven by Ekman transport, and a large stratocumulus cloud deck capped by a strong inversion layer (Bretherton et al., 2004). The inversion confines surface-derived scalars to the MBL, separated from the stable, dry, and relatively quiescent FT. The stratocumulus topped MBL is shallow near the coast (∼1 km) with more broken clouds. Away from shore, the MBL deepens with thicker clouds and more extensive precipitation in the form of drizzle. Satellite observations show frequent hundred-kilometer sized openings in the stratocumulus cloud deck. Termed “pockets of open cells” (POCs), these features persist for a timescale of a day and advect with the mean wind (Stevens et al., 2005). The geographical gradient in cloud properties as well as the formation and evolution of POCs likely depend on the availability of aerosols that can act as CCN and suppress drizzle, and drizzle that in turn removes said aerosols. The coastal regions of Chile and Peru are influenced by pollution emissions of SO_4^{2-} and SO_2 from fossil fuel consumption and processing of copper ores. Because the prevailing wind direction at the surface is S/SE along the Andes mountain range, anthropogenic influence decreases quickly away from shore, where a greater contribution to the SO_4^{2-} burden and larger fraction of CCN likely originate from DMS.

ACPD
11, 2873–2929, 2011

In this paper, we will look at the longitudinal distributions of SO_2 and SO_4^{2-} in VOCALS-REx to evaluate the impact of coastal pollution on the SEP. To assess the importance of entrainment relative to surface sources, we will focus on the vertical profiles of gases and aerosols from the aircraft for the remote region. Finally, following up on the DMS budget presented in Yang et al. (2009), we will examine the diel budgets of SO_2 and SO_4^{2-}.

2 Experimental

During VOCALS-REx in 2008 (Wood et al., 2011), the National Oceanographic and Atmospheric Administration (NOAA) ship *Ronald H. Brown* (*RHB*) was in the SEP from 20 October to 3 Novenber and from 10 November to 11 December. The ship made multiple transects between the coastal city of Arica at 70° W and the remote marine region near the Woods Hole Oceanographic Institution (WHOI) Improved Meteorology (IMET) moored buoy at 20° S, 85° W. The National Science Foundation (NSF)/National Center for Atmospheric Research (NCAR) aircraft C-130 flew 14 research flights (RF) out of Arica between 15 October and 15 November. Eight flights were dedicated to survey the 20° S line to as far as 86° W, four were designed to study the structures and evolution of POCs, and two were parallel to the coast between 20° S and 30° S. For the 20° S surveying flights, the aircraft typically flew 10-min level legs near the surface, in the mid MBL, at cloud level, and above clouds. Sounding profiles from the surface to ~4 km were frequently performed.

2.1 *RHB*

The measurements of atmospheric DMS concentration at 20 Hz and hourly sea-to-air flux by eddy covariance during VOCALS-REx were outlined by Yang et al. (2009). Instrument design and flux computation were detailed by Blomquist et al. (2010). Seawater DMS was taken from the ship's non-toxic water supply at ~5.5 m below the ocean

ACPD
11, 2873–2929, 2011

surface, extracted by a purge-and-trap method, and analyzed by gas chromatography with a sub-nM detection limit every 15 ~ 30 min (Bates et al., 2000).

Aerosol chemical compositions and size distributions were measured by the Pacific Marine Environmental Laboratory through an isokinetic inlet on the forward deck of the ship. Submicron and supermicron aerosols were collected on a two-stage multi-jet cascade impactor (50% aerodynamic cutoff diameters of 1.1 and 10 µm) over 2 ~ 23 h. In addition to providing gravimetric mass, collected aerosols were analyzed for soluble concentrations of sodium (Na^+), potassium (K^+), calcium (Ca^{2+}), magnesium (Mg^{2+}), ammonia (NH_4^+), methane sulfonate (MSA^-), chloride (Cl^-), bromide (Br^-), nitrate (NO_3^-), sulfate, and oxalate (Ox^{2-}) using ion chromatography (Bates et al., 2008). Non-sea-salt-SO_4^{2-} and Cl^- deficit were calculated by subtracting sea-salt components from total concentrations. An Aerodyne quadrupole aerosol mass spectrometer (Q-AMS) was used to continuously measure submicron particulate concentrations of SO_4^{2-}, NO_3^-, NH_4^+, and organic matter (Hawkins et al., 2010). The AMS quantified non-refractory aerosols (those vaporizing at 600 °C), thus excluded mineral dust, elemental carbon, and sea-salt. AMS sulfate agreed exceptionally well with collocated submicron filter measurements of SO_4^{2-} (slope of 1.09 and r^2 of 0.88) and showed a high degree of correlation with integrated submicron aerosol volume (r^2 of 0.86). Aerosol size distributions from 0.02 ~ 10 µm were obtained by merging spectra from a differential mobility particle sizer and an aerodynamic particle sizer at a regulated RH of 60% (Bates et al., 2008). Except for filter samples, above measurements were reported at 5-min intervals.

The inversion height (Z_i) was determined from radiosondes launched every six hours from the ship by the NOAA Earth System Research Laboratory (de Szoeke et al., 2008). During the second half of VOCALS-REx, cloud fraction and cloud top height were determined from a W-band radar. Precipitation rate was continuously estimated by a shipboard optical rain gauge. The surface-based mixed layer height (MLH), useful for determining coupling and decoupling, was estimated hourly from a High Resolution Doppler Lidar (2 µm) from velocity variance (turbulence) profiles and aerosol

ACPD
11, 2873–2929, 2011

backscatter gradient (Tucker et al., 2009). The vertically-integrated liquid water content, or liquid water path (L_{WP}), was estimated at 10-min intervals from a two-channel microwave radiometer by University of Miami using a physical retrieval similar to Zuidema et al. (2005) that takes cloud temperature into account.

2.1.1 C-130

DMS and SO_2 were measured at 1 Hz using an atmospheric pressure ionization mass spectrometer at a pptv detection limit by Drexel University (Bandy et al., 2002; Thornton et al., 2002). Both DMS and SO_2 on the C-130 were sampled from backward facing inlets that should not be affected by cloud droplets. Within clouds, measurements of those gases represented interstitial concentrations.

The University of Hawaii aerosol instruments were typically located behind a low turbulence inlet (LTI) (Huebert et al., 2004). Breaking up of cloud droplets upon collision on the wall of the inlet caused a cloud shattering artifact, or an increase in the measured number of particles. By excluding such incidents, aerosol data at cloud level were biased towards cloud free regions. A high resolution time-of-flight AMS on the C-130 measured aerosol concentration of SO_4^{2}, NO_3^{-}, NH_4^{+}, and organic matter every 10 s. As with the AMS on the ship, the AMS on the C-130 sampled with a near-unity efficiency for aerosols up to ~0.8 µm in diameter and excluded large particles.

Aerosol size distributions at dried RH of ~ 20% from diameters of 0.01 to 10 µm were obtained at 1-min intervals by merging spectra from a radial differential mobility analyzer (0.01 ~ 0.20 µm), a TSI long differential mobility analyzer (0.10 ~ 0.50 µm), a PMS laser optical particle counter (0.12 ~ 8.0 µm), and a TSI 3321 aerodynamic particle sizer (0.78 ~ 10.0 µm) (Howell et al., 2006). Direct comparisons between the distributions measured on the C-130 and *RHB* can only be qualitative in nature because of the different sampling strategies and airspeeds. At the dried environment of C-130 measurements, MBL aerosols had most likely undergone efflorescence and been approximately halved in size, whereas the already dry FT aerosols remained largely unchanged. The *RHB* distributions, on the other hand, were measured at ~60% RH,

ACPD
11, 2873–2929, 2011

closer to the ambient RH of ~70% and above the humidity threshold for efflorescence; the measured diameters were thus only ~10% smaller than ambient diameters.

Bulk cloud water was collected by Colorado State University every ~10 min with an Airborne Cloud Collector (Straub and Collett Jr., 2004; Straub et al., 2007), which had a 50% size cut diameter of 8 µm and thus collected most cloud drops but excluded small, unactivated aerosols. Cloud water was analyzed for pH, SO_2, H_2O, HSO_3^-, and SO_3^{2-} (together $S(IV)$), peroxides, etc. Details of cloud water sampling and analysis during VOCALS-REx are provided in Benedict et al. (2011). Aqueous cloud solute concentrations in µM can be converted to atmospheric mixing ratios using cloud liquid water content (L_{WC}) measured by a Gerber Scientific Particulate Volume Monitor.

Inversion heights determined based on potential temperature and dew point gradients from the C-130 sounding showed excellent agreement with those determined from potential temperature profiles from shipboard radiosondes. Because Z_i varied both with longitude and with the time of day, to average vertical distributions, altitude (Z) is normalized to Z_i, with $Z/Z_i = 1$ indicating the inversion. For FT averages along 20° S, only observations within 1 km above Z_i are included.

3 Observations

We separate the VOCALS-REx sampling area longitudinally to the "near shore" (70° W ~ 73° W) and "offshore" regions (73° W ~ 86° W). We further isolate the "remote" region (78° W ~ 86° W) from the offshore region. Figure 1 shows the *RHB* cruise track color-coded by the DMS sea-to-air flux; the dotted and solid lines indicate the offshore and remote regions. This stratification is based on aircraft observation of CO and shipboard measurement of radon, both indicators of continental influence. The lowest MBL CO concentration was found west of 78° W at ~62 ppbv; CO increased to ~73 ppbv near the coast as a result of combustion, corresponding to elevated SO_4^{2-} concentrations. Hawkins et al. (2010) showed that the concentration of radon (a radioactive decay product of uranium in rocks and soil) in the remote marine region was

ACPD
11, 2873–2929, 2011

approximately half of the value by the coast. Three-day back trajectories by those authors showed that east of 75° W, airmasses had been previously in contact with land south of the VOCALS-REx sampling area, near the Chilean capital Santiago. In contrast, west of 78° W, air had originated from the remote South Pacific. Figure 2 show a typical 20° S survey flight by the C-130 (RF 03 on 21 October). The flight track is color-coded by SO_2 concentration, with marker size corresponding to SO_4^{2-}. The aircraft encountered more polluted air in two flights south of ∼22° S, closer to Santiago, as well as on RF 14. Greater continental influence was also observed on the *RHB* north of ∼15° S, closer to Peru. For our "20° S" averages, we limit the latitudinal range to 18° S ∼ 22° S and exclude RF 14 from C-130 statistics. Because the aircraft usually took off from Arica in the early morning, reached 80 ∼ 85° W at around sunrise, and returned to shore in the afternoon, spatial and temporal biases are inherent. We will thus mostly rely on ship observations for diel cycles and aircraft observations for vertical structures.

3.1 Longitudinal distributions

It was hypothesized prior to VOCALS-REx that coastal upwelling of cold, nutrient rich water stimulates growth of phytoplankton, which should lead to more seawater and hence atmospheric DMS at the coast than in the remote region. We only observed enhanced seawater DMS in isolated pockets near shore. More often high seawater DMS was associated with the edge of an eddy or near a front between two water masses, where temperature and salinity changed markedly. On average along 20° S, seawater DMS was not substantially different between the coastal and the remote regions. Higher atmospheric DMS concentration and sea-to-air flux were observed away from the coast principally as a result of higher wind speed. At the same air-sea concentration difference in DMS (dictated by the seawater concentration), a higher wind speed generally leads to a greater transfer velocity, and hence more DMS flux out of the ocean (Huebert et al., 2004; Yang et al., 2011).

ACPD
11, 2873–2929, 2011

Project average concentrations of DMS, SO_2 and SO_4^{2-} along 20° S and in the MBL and FT are shown in Fig. 3. Pollution emission was unquestionably the major source of sulfur mass near shore, with SO_2 and SO_4^{2-} concentrations elevated at ~80 and ~800 pptv in the MBL, respectively. Moving offshore towards the remote region, SO_2 and SO_4^{2-} decreased rapidly to "background" levels. SO_2 varied from flight to flight but was relatively well mixed with a mean (1 sigma) MBL concentration of ~25 (15) pptv, about 40% of the DMS concentration measured on the ship. We show later that the relatively low concentration of SO_2 in the MBL was likely due to processing of air by stratocumulus clouds. SO_4^{2-} concentration was quite variable horizontally and vertically, which in part explains the difference between the averaged MBL concentrations from the *RHB* 118 (85) pptv and C-130 60 (60) pptv in the remote MBL.

3.2 Vertical structures away from shore

The mean C-130 vertical profiles of temperature, dew point, potential temperature, L_{WC}, CO, O_3, DMS, SO_2, and SO_4^{2-} for the offshore region before sunrise are shown in Fig. 4. The elevated L_{WC} and sharp gradients in temperatures and dew point clearly indicate the inversion ($Z/Z_i = 1$). The C-130 DMS concentration averaged zero in the FT, and appeared to be somewhat lower than that measured from the ship in the MBL for reasons that are not clear at the moment. Tracers with sources in the FT (CO, O_3) showed increasing concentrations with Z/Z_i, while the opposite was true for tracers mostly originated from the surface (sulfur species). Figure 5 shows the mean aerosol size distributions (number, surface area, and volume) from the C-130 in the remote region, stratified by Z/Z_i. The low ($Z < 0.2Z_i$; $N = 220$) and mid ($0.4Z_i < Z < 0.7Z_i$; $N = 86$) MBL distributions were similar, with the Hoppel minimum at ~70 nm indicating cloud processing. The upper MBL distribution ($0.8Z_i < Z < Z_i$; $N = 493$) as well as cloud level SO_4^{2-} concentration in Fig. 4 were biased towards cloud free and POC regions, as cloud shattering compromised measurements inside of clouds. A greater number of small particles was seen in the upper MBL, likely related to new particle nucleation.

ACPD
11, 2873–2929, 2011

The above cloud distribution ($1.1Z_i < Z < 1.3Z_i$; $N = 365$) was a superposition of two modes: a 30 nm background mode associated with low CO ($<\sim 64$ ppbv) and an 80 nm mode associated with high CO ($>\sim 74$ ppbv) that indicates long distance transport of pollution.

3.3 Diurnal cycles

Turbulence at the inversion irreversibly entrains air from the FT into the MBL, with the rate of entrainment varying with radiative fluxes at the stratocumulus cloud-top. At night, longwave cooling causes greater convective instability, more turbulent mixing in the MBL, and increased entrainment (Lilly, 1968). During the day, shortwave heating of the cloud-top partially suppresses turbulence in the MBL, which reduces entrainment and causes the surface and the upper MBL to become decoupled (Nicholls, 1984). Evaporative cooling from falling drizzle droplets may further affect mixing in the MBL.

An array of measurements from the *RHB* during VOCALS-REx illustrated the diel cycling of the MBL (Fig. 6). Vertical velocity profiles and MLH from the shipboard Lidar indicated a coupled MBL at night; as the instrument only reported MLH up to the cloud bottom, this measurement was generally an underestimate of the actual height of the well-mixed layer in the nighttime. Lidar measurements showed that the average velocity variance in the MBL was ~50% lower during the daytime, with MLH only reaching $60 \sim 70\%$ of Z_i in the remote region, generally below the stratocumulus cloud bottom but above the lifting condensation level (LCL). While a cloud base well above the LCL is usually thought to indicate decoupling, the turbulence-based MLH measurement provides more direct information on whether surface-based measurements are applicable up to Z_i. Cloud fraction from the W-band radar averaged over 90% between midnight and sunrise and decreased to $20 \sim 30\%$ in the afternoon. L_{WC} peaked above 150 g m^{-2} over the same time span, more than three times the afternoon value. The optical rain detected sporadic precipitation events upto ~1 mm h^{-1}, but typically at a lower value of ~0.2 mm h^{-1}. Precipitation was more intense and frequent offshore, with most of the detectable rain events taking place west of 80° W.

ACPD
11, 2873–2929, 2011

Surface concentrations of chemical tracers are also affected by the alternating MBL dynamics. O_3 averaged 26 (*RHB*) and 52 ppbv (C-130) below and above Z_i, respectively, with pronounced variability in the MBL. At night, O_3 built up as a result of entrainment from the FT, whereas during the day, O_3 decreased steadily because photolysis and heterogeneous reactions outpaced entrainment. Deposition to the ocean surface represents a small but continuous sink for O_3 at all times. As with the DMS budget (Yang et al., 2009), we can estimate the entrainment velocity (ω_e) by balancing the nighttime O_3 build up in the MBL with entrainment and deposition fluxes, assuming no chemical source and loss at night (Clarke et al., 1996). Adopting a deposition velocity of 0.01 cm s^{-1} (derived from eddy covariance measurements of O_3 during the Stratus 06 cruise in the SEP, J. Hare, personal communication, 2010), we calculate a nighttime ω_e of ~6 mm s^{-1}, higher than that derived from the DMS budget (4 mm s^{-1}). Using a greater deposition velocity would require an even higher ω_e to balance the O_3 budget. However, O_3 was generally higher in the north (~30 ppbv at 19° S) than in the south (~20 ppbv at 21° S), implying a gradient along the mean wind. Thus the advective flux of O_3 could be substantial and complicate the interpretation of ω_e from the O_3 budget.

SO_4^{2-} concentrations measured by the AMS on the *RHB* displayed large diel variability, as exemplified by the period from 28 October to 31 October when the ship was steaming eastward at 11 knots from 85° W to 75° W (Fig. 7). SO_4^{2-} increased from 20 ~ 30 pptv to over 150 ~ 300 pptv over the first few hours after sunset, peaking at around 04:00 UTC (01:00 a.m. local), with O_3 showing a similar trend. SO_4^{2-} then declined over the rest of the day, with the sharpest decrease in the early morning, when the precipitation peaked (~0.3 mm h^{-1}) and the MBL started to become decoupled, as evidenced from the difference between the Z_i and MLH. The rapid nighttime increase in SO_4^{2-} is in contrast with previous measurements in the Equatorial Pacific (Huebert et al., 1996), which showed a daytime build up of SO_4^{2-} from SO_2 oxidation by OH. Moreover, the observed build up in SO_4^{2-} is much too fast to be caused by any chemical mechanisms alone. As O_3 was increasing at the same time, the most likely explanation evokes a SO_4^{2-} source above, such as in-cloud oxidation of SO_2. This source could

ACPD
11, 2873–2929, 2011

not significantly increase the surface concentration during the day due to decoupling of the MBL. As the MBL became recoupled after sunset, air rich in SO_4^{2-} was mixed downwards, increasing the surface concentration. Precipitating droplets that evaporate while falling return aerosols to the MBL, but likely at greater sizes than before being scavenged. This process could further speed up the transport of SO_4^{2-} from cloud level to the surface. Unfortunately, per flight plans, the C-130 did not sample the remote region at this time of the day to directly verify this proposed mechanism.

The observed diel variability in AMS SO_4^{2-} is consistent with size distribution measurements on the *RHB*, which are stratified according to the time of day in Fig. 8. In the remote region, the largest accumulation mode was measured in the evening (22:00 ~ 06:00 UTC; N = 1455). The nuclei and coarse modes appeared to be larger in the late afternoon (1400 ~ 2200 UTC; N = 1478) than in the early morning (06:00 ~ 14:00 UTC; N = 1488), presumably due to photochemistry and the slightly higher winds during the day, respectively.

4 Discussion

To better understand the natural sulfur cycling in the SEP, let us look at the budgets of different sulfur species in the remote region. The conservation equation for any chemical species, S, in the MBL is represented below, with the overbar representing an average in time and/or space:

$$\frac{\partial \overline{S}}{\partial t} + \overline{u}\frac{\partial \overline{S}}{\partial x} + \frac{\partial \overline{S'w'}}{\partial z} = P - L \quad (1)$$

The terms on the LHS are the time-rate of change in the concentration of S, horizontal advection due to gradients along the mean wind, and vertical flux divergence, respectively. In situ production and loss of S are represented by P and L on the RHS.

In the following sections, we will first briefly introduce and approximate each of the rates in the budget equations of SO_2 and SO_4^{2-}. In the end, we will estimate the diel

ACPD
11, 2873–2929, 2011

cycles of SO_2 and SO_4^{2-} based on those rates and adjust the least certain terms if necessary to achieve mass balance. Through multi-variate fitting, Yang et al. (2009) showed that the horizontal gradient in atmospheric DMS concentration mostly lay in the E-W direction, orthogonal to the prevailing wind along the Andes (~150°); the advective flux of DMS was thus negligible. While DMS was not measured in the upwind region of the SEP during the campaign, previous observations of seawater DMS in the South Pacific (e.g. Lee et al., 2010) were similar to those measured during VOCALS-REx, implying that the biogenic sulfur source strength in the upwind region was likely not very different. Analogous multi-variate analysis of SO_2 and SO_4^{2-} concentrations in the remote MBL over the entire project resulted in similarly small advective fluxes on average because gradients in SO_2 and SO_4^{2-} were also largely longitudinal. We will therefore ignore advection in the calculations below.

4.1 Sulfur dioxide budget

Observations from the Equatorial Pacific first demonstrated a quantitative anti-correlation between DMS and SO_2 as a result of the oxidation of DMS by the OH radical (Bandy et al., 1996). Integrating Eq. (1) from the surface to Z_i for SO_2 leads to:

$$\frac{\partial \left\langle \overline{SO_2} \right\rangle}{\partial t} = F_{SO_2,0} - F_{SO_2,Z_i} + \left\langle P_{SO_2} \right\rangle - \left\langle L_{SO_2,OH} \right\rangle - \left\langle L_{SO_2,cloud} \right\rangle - \left\langle L_{SO_2,aero} \right\rangle \quad (2)$$

Here angular brackets denote column integrals, with every term now in units of flux (e.g. μmoles m^{-2} day^{-1}). Flux divergence is separated into the first and second terms on the RHS, representing the SO_2 flux at the ocean surface (deposition) and at Z_i (entrainment). P_{SO_2} is in situ production of SO_2 from DMS, while the last three terms represent losses due to OH, in clouds, and in aerosols, respectively.

ACPD
11, 2873–2929, 2011

4.1.1 SO_2 dry deposition

The surface flux, or the dry depositional loss, of SO_2 to the ocean may be related to the SO_2 concentration near the surface ($[SO_{2,0}]$) and a deposition velocity (V_{dep}):

$$F_{SO_2,0} = -V_{dep}[SO_2,0] \quad (3)$$

The seawater concentration is irrelevant here for the air-sea exchange of SO_2 due to its high reactivity in the seawater (Fairall et al., 2007). At a typical VOCALS-REx wind speed of $6\,m\,s^{-1}$, models based on atmospheric resistance predict $V_{dep} \approx 5\,mm\,s^{-1}$ (Wesely and Hicks, 1977; Fairall et al., 2007). Aircraft eddy covariance measurements from a recent Equatorial project yielded a somewhat lower V_{dep} of $3 \sim 4\,mm\,s^{-1}$ at this wind speed (Faloona et al., 2010). With $V_{dep} = 4 \pm 1\,mm\,s^{-1}$ and $[SO_{2,0}] = 35\,pptv$, the dry deposition flux was $0.6 \pm 0.1\,\mu mole\,m^{-2}\,day^{-1}$, or $0.4 \pm 0.1\,pptv\,h^{-1}$ for a 1.3 km deep MBL. We will show later that dry deposition was a minor term in the SO_2 budget, such that the uncertainty in V_{dep} does not significantly alter our conclusions.

4.1.2 SO_2 entrainment

The entrainment of SO_2 may be formulated as the entrainment velocity, ω_e, multiplied by the concentration jump in SO_2 across the inversion (Lilly, 1968), with Z_i^- and Z_i^+ indicating below and above Z_i:

$$F_{SO_2,Z_i} = \omega_e\{[SO_2,Z_i^-] - [SO_2,Z_i^+]\} \quad (4)$$

From the nighttime budget analysis of DMS in the offshore region, Yang et al. (2009) estimated an ω_e of $\sim 4\,mm\,s^{-1}$, matching the diel mean estimated from climatological and mixed-layer models for this region (Wood and Bretherton, 2004; Caldwell et al., 2005). Using the Weather and Research Forecast model and solving for the change of MBL depth over time, Rahn and Garreaud (2010) derived a similar mean ω_e value as the residual for VOCALS-REx.

ACPD
11, 2873–2929, 2011

With a mean of ∼25 pptv from the C-130, the concentration of SO_2 in the remote MBL was higher in the day (30 ∼ 50 pptv) than before sunrise (∼20 pptv) due to DMS oxidation. The concentration at cloud level was reduced to ∼18 pptv, likely due to a combination of in-cloud oxidation and incorporation of FT air by entrainment. At ∼26 pptv, SO_2 in the FT likely originated from long distance transport of anthropogenic and natural emissions. Using a mean ω_e of 4 mm s^{-1} and the concentration jump between the FT and the cloud level (26 and 18 pptv), entrainment increased MBL SO_2 burden at an approximate rate of 0.1 µmole m^{-2} day^{-1}, or ∼0.1 pptv h^{-1}.

However, as entrainment is a unidirectional process, the "mass flux" of SO_2 mixed into the MBL from the FT does not depend on the concentration below the inversion. Multiplying 4 ± 2 mm s^{-1} by the FT concentration then yields a SO_2 mass flux of $\sim 0.3 \pm 0.2$ µmole m^{-2} day^{-1}, all of which would be converted to SO_4^{2-} aerosols, mostly in clouds as we will show later.

4.1.3 SO_2 production from DMS

DMS is principally oxidized by OH in two separate pathways: H-atom abstraction and OH-addition (Yin et al., 1990). The abstraction channel is favored at high temperatures and essentially all leads to SO_2, while the addition channel speeds up at low temperatures and leads to MSA, dimethylsulfoxide (DMSO), and also SO_2. From the DMS budget, Yang et al. (2009) estimated a diel mean effective OH concentration of $1.4 \pm 0.2 \times 10^6$ OH molecules cm^{-3}, peaking at $\sim 5 \times 10^6$ molecules cm^{-3} at noontime. Representing the conversion efficiency from DMS to SO_2 as γ, which typically ranges from 0.6 ∼ 0.9 and is recommended to be 0.7(±0.2) by Faloona (2009), the in situ production of SO_2 is:

$$\left\langle P_{SO_2} \right\rangle = \gamma (k_{OH+DMS}[OH] \left\langle \overline{DMS} \right\rangle) \quad (5)$$

Here k_{OH+DMS} is the total second order rate constant of the DMS-OH reaction (sum of the abstraction and addition channels). At an average MBL temperature of ∼13 °C

ACPD
11, 2873–2929, 2011

in VOCALS-REx, $k_{OH} \approx 7.9 \times 10^{-12}$ cm^3 molec^{-1} s^{-1}, with the abstraction pathway accounting for 60% of the total oxidation (Sander et al., 2006).

MSA largely resides in the particulate phase; in VOCALS-REx, most of the MSA was found in the fine mode according to filter measurements. Since MSA is entirely produced from DMS whereas SO_4^{2-} can have both natural and anthropogenic origins, the MSA:SO_4^{2-} ratio can be used to infer branching in DMS oxidation as well as the natural contribution to the sulfur burden (Bates et al., 1992). The submicron MSA:SO_4^{2-} ratio in this study varied between 0.04 ~ 0.15 (mean of 0.08) and closely followed the DMS concentration (Fig. 9). If MSA was the only other major oxidation product of DMS besides SO_2 (and ultimately SO_4^{2-}), and if all of the SO_4^{2-} in the remote region was formed from DMS, assuming equal lifetime for MSA and SO_4^{2-} due to precipitation scavenging implies $\gamma \approx 0.9$ for a MSA:SO_4^{2-} ratio of 0.1. Accounting for DMSO, the other major product from the addition channel but not measured during the campaign, would reduce γ. Using a range of 0.7 ~ 0.9 in γ led to a diel average SO_2 gas phase production of 2.2 ~ 2.8 μmoles m^{-2} day^{-1}, or 1.8 ~ 2.3 pptv h^{-1}. In midday, the SO_2 production rate from DMS peaked at 7.5 ~ 9.7 μmoles m^{-2} day^{-1}, or 6.1 ~ 7.8 pptv h^{-1}.

4.1.4 SO_2 gas phase oxidation

The rate of daytime oxidation of SO_2 by OH is:

$$\left\langle L_{SO_2,OH} \right\rangle = k_{OH+SO_2}[OH]\left\langle \overline{SO_2} \right\rangle \quad (6)$$

The second order rate constant between OH and SO_2, k_{OH+SO_2}, is about 9.6×10^{-13} cm^3 molec^{-1} s^{-1} at ~13 °C (Sander et al., 2006). At a SO_2 concentration of 35 pptv, the diel loss rate was 0.22 μmoles m^{-2} day^{-1}, or 0.17 pptv h^{-1}. The greatest SO_2 loss occurred at a rate of 0.9 μmoles m^{-2} day^{-1}, or 0.7 pptv h^{-1}, not in midday, but in the late afternoon.

ACPD
11, 2873–2929, 2011

4.1.5 SO_2 aqueous phase oxidation – in cloud

With extensive cloud coverage in the SEP, in-cloud oxidation is expected to be a major sink for SO_2 and source of SO_4^{2-}. Figure 10 shows SO_2 concentration below Z_i vs. L_{WC} for the offshore region. Compared to the concentration below or outside of clouds, the interstitial SO_2 concentration was reduced to ~18 pptv, with perhaps slightly higher concentration during the day than at night. In an aqueous solution, SO_2 is equilibrated to $SO_2.H_2O$, HSO_3^-, and SO_3^{2-}:

$$[SO_2 \cdot H_2O] = H_{SO_2}[SO_2] \tag{7}$$

$$[HSO_3^-] = \frac{K_{s1}[SO_2 \cdot H_2O]}{[H^+]} = \frac{H_{SO_2}K_{s1}[SO_2]}{[H^+]} \tag{8}$$

$$[SO_3^{2-}] = \frac{K_{s2}[HSO_3^-]}{[H^+]} = \frac{H_{SO_2}K_{s1}K_{s2}[SO_2]}{[H^+]^2} \tag{9}$$

The Henry's coefficient $H_{SO_2} = 1.23\,M\,atm^{-1}$, equilibrium constants $K_{s1} = 1.3 \times 10^{-2}$ M, and $K_{s2} = 6.6 \times 10^{-8}$ M at 298 K all increase at lower temperatures with $-\Delta H/R$ of 3135, 1960, and 1495 K, respectively (Hoffmann and Calvert, 1985). K at the ambient temperature is related to that at 298 K (K_{298}) by the relationship $K = K_{298}\exp[-\Delta H/R(1/T - 1/298)]$).

In the remote region, with an average cloud water H_2O_2 concentration of 65 µM, or ~0.9 ppbv in the gas phase (Benedict et al., 2011), stoichiometrically there was enough oxidant to oxidize all of the $S(IV)$ to SO_4^{2-}. Bulk cloud water measurements showed mean SO_4^{2-} concentration of ~45 µM in the remote region (Benedict et al., 2011), which at $L_{WC} \approx 0.2\,g\,m^{-3}$ converts to ~200 pptv, higher than the below cloud concentration. $S(IV)$, on the other hand, was barely detectable in cloud water. Cloud water had an average pH of 4.2 (Benedict et al., 2011), consistent with the ensemble mean pH of 4.3

ACPD
11, 2873–2929, 2011

in stratocumulus droplets from a recent a survey of measurements over the last twenty years (Faloona, 2009). At this pH, HSO_3^- is the predominant $S(IV)$ species.

Ignoring mass transfer limitation, the loss rate of $S(IV)$, and hence the production rate of SO_4^{2-}, by reaction with H_2O_2 can be estimated according to Martin and Damschen (1981) [$M\,s^{-1}$]:

$$-\frac{d[S(IV)]_{H_2O_2}}{dt} = k_{H_2O_2}[H^+][H_2O_2][HSO_3^-] \quad (10)$$

$$k_{H_2O_2} = \frac{2.1\times10^6}{0.1+[H^+]} \quad (11)$$

The rate constant $k_{H_2O_2}$ [$M^{-2}\,s^{-1}$] decreases at lower temperatures with $-\Delta H/R = -3650$ (Maahs, 1983). The reaction is largely pH insensitive because $[H^+]$ in Eqs. (7b) and (8a) cancel. With a gas phase SO_2 concentration of 25 pptv, cloud water H_2O_2 concentration of 65 µM (0.9 ppbv), and pH of 4.2, the instantaneous loss rate of $S(IV)$ due to H_2O_2 is $7.2\times10^{-10}\,M\,s^{-1}$. An alternate reaction rate by Hoffmann and Calvert (1985) is about three times higher than the one from Martin and Damschen (1981). We demonstrate later that this alternate rate appears to be unrealistically high from the perspective of the steady state mass balance of SO_2.

The loss rate of $S(IV)$ by reaction with O_3 [$M\,s^{-1}$] is:

$$-\frac{d[S(IV)]_{O_3}}{dt} = (k_{O_3,0}[SO_2\cdot H_2O] + k_{O_3,1}[HSO_3^-] + k_{O_3,2}[SO_3^{2-}])[O_3] \quad (12)$$

where $k_{O_3,0}$, $k_{O_3,1}$, and $k_{O_3,2}$ are 2.4×10^4, 3.7×10^5, and $1.5\times10^9\,M^{-1}\,s^{-1}$ at 298 K, respectively (Hoffmann, 1986). Because $k_{O_3,2}$ is orders of magnitude higher than the other two reactions, the overall reaction rate approximately varies inversely with the square of $[H^+]$ and is greatly enhanced at high pH when there is more SO_3^{2-}. At the average cloud pH and gas phase O_3 concentration of 26 ppbv, the instantaneous loss rate of $S(IV)$ due to O_3 is $\sim4\times10^{-12}\,M\,s^{-1}$, two orders of magnitude slower than the H_2O_2

ACPD
11, 2873–2929, 2011

reaction. Benedict et al. (2011) examined rates of aqueous $S(IV)$ oxidation by H_2O_2, by O_3, and by O_2 (catalyzed by Fe and Mn) and found that H_2O_2 was the dominant oxidant in most cases, except where pH exceeded approximately 5.5.

The aqueous phase oxidation rate of $S(IV)$ in cloud [$M\,s^{-1}$] can be converted to an equivalent gas phase rate of SO_2 loss [$pptv\,h^{-1}$] using L_{WC}:

$$L_{SO_2,cloud} = 3.6 \times 10^9 L_{WC} RT \left(-\frac{d[S(IV)]_{H_2O_2}}{dt} - \frac{d[S(IV)]_{O_3}}{dt}\right) \quad (13)$$

R is the gas constant ($0.082\,atm\,L\,K^{-1}\,mole^{-1}$), and T is the average cloud temperature (~282 K). Under the scenario above, $L_{SO_2,cloud}$ is $12\,pptv\,h^{-1}$ ($48\%\,h^{-1}$).

However, using the instantaneous $d[S(IV)]/dt$ (i.e. assuming an open system) to budget SO_2 loss over time will certainly lead to an overestimation. In a more realistic closed system, without replenishment, the concentration of the limiting reactant decreases significantly as reaction proceeds, and so will $d[S(IV)]/dt$. To calculate SO_2 depletion as a function of time in cloud, we start initially with 25 pptv of SO_2, 0.9 ppbv of H_2O_2, L_{WC} of $0.2\,g\,m^{-3}$, and T of 282 K. For simplicity, since there is more than sufficient H_2O_2 to oxidize all of the SO_2 and this reaction is largely pH-independent, a constant pH of 4.2 and an O_3 concentration of zero are applied. We also assume rapid equilibration between the gas phase and aqueous phase (i.e. no mass transfer limitation). As seen in Fig. 11, 9.3 pptv (37%) of SO_2 is consumed after an hour in cloud, which is 0.8 times the rate calculated from the open system.

From large eddy simulations (LES), Feingold et al. (1998) showed that for a stratocumulus capped MBL, a parcel of air is in clouds for on average ~15 min in an hour. From Fig. 11, 2.8 pptv of SO_2 (~11%) is oxidized to SO_4^{2-} after 15 min, or 1.9 pptv if we account for the mean cloud fraction of ~0.67. The SO_2 formation rate from DMS is $1.8 \sim 2.3\,pptv\,h^{-1}$ (for γ of $0.7 \sim 0.9$) on a diel average. Adding $\sim 0.1\,pptv\,h^{-1}$ due to entrainment and subtracting dry deposition at $0.4\,pptv\,h^{-1}$ and OH loss at $\sim 0.2\,pptv\,h^{-1}$ leaves a daily residual of $1.3 \sim 1.8\,pptv\,h^{-1}$. Thus the approximated loss rate of SO_2 in clouds appears comparable to the production rate. If using the much higher rate

ACPD
11, 2873–2929, 2011

constant of the SO_2-H_2O_2 reaction from Hoffmann and Calvert (1985) instead, the in-cloud oxidation of SO_2 would far exceed the production from DMS, which is unrealistic and inconsistent with observations. While the rate constant from Martin and Damschen (1981) appears to be more applicable for VOCALS-REx, the large discrepancy in this reaction rate contributes to the uncertainty of our budget estimates.

In addition, ignoring mass transfer and using mean bulk cloud water parameters may contribute to caveats in the calculations above. Mass transfer from interstitial air to a cloud droplet involves diffusion in the gas phase, interfacial transfer from the gas to the aqueous phase, and diffusion in the aqueous phase. If the rate of the chemical reaction is faster than any of those steps, a gradient in concentration develops away from the interface and the reaction becomes limited by mass transfer. The typical mean cloud droplet radius was $10 \sim 15\,\mu m$ in the VOCALS-REx remote region from MODIS images. Schwartz (1988) showed that even for 30 µm diameter cloud droplets, in-cloud reaction between SO_2 and H_2O_2 does not appear to be limited by mass transfer. However, both the temperature and the cloud droplet size change significantly during the cloud lifetime. Thus calculations assuming instantaneous equilibrium between the gas and aqueous phase and overly simplified physical conditions should be considered rough estimates.

Zhang et al. (1999) modeled the depletion of SO_2 by H_2O_2 in a case of excess oxidants within a single cloud pass using LES coupled with chemistry. While our calculated depletion of SO_2 is slower than the estimate from Zhang et al. (1999) because they used the H_2O_2 rate constant from Hoffmann and Calvert (1985), qualitatively the results are similar. Those authors also suggested that SO_4^{2-} produced by the oxidation of H_2O_2 is evenly distributed across the drop-size spectrum and tends to broaden the processed CCN spectrum, which can enhance coalescence and hence drizzle. From our calculation, it appears that in-cloud oxidation was enough to account for essentially all of the SO_2 loss, which would render other sinks insignificant. Nevertheless, we will look at the oxidation of SO_2 in sea-salt aerosols for the sake of completeness.

ACPD
11, 2873–2929, 2011

4.1.6 SO_2 aqueous phase oxidation – in sea-salt aerosols

As alluded to previously, the oxidation of SO_2 by O_3 only becomes important at pH $>\sim 5.5$. While aerosol pH was not directly measured during VOCALS-REx, we can get a sense for the acidity of the aerosol phase by looking at filter measurements on the *RHB*. From ion balance of aerosols, the anion:cation molar equivalent ratio averaged 1.38:1 for the fine mode away from shore, implying acidic aerosols. As $60 \sim 70\%$ of the total aerosol surface area near the ocean surface was submicron, the fine mode was acidic due to the uptake of SO_2, SO_4^{2-}, etc. The anion:cation ratio peaked above 2.3:1 (most acidic) when the ship was near shore, where SO_4^{2-} and NO_3^- levels from pollution were elevated. This longitudinal pattern anion:cation ratio is in agreement with shipboard AMS measurements of submicron SO_4^{2-} and NH_4^+ (Fig. 12). SO_4^{2-} in aerosols is typically titrated by ammonium (NH_4^+), which can have continental and marine sources (Zhuang and Huebert, 1996), to form ammonium bisulfate (NH_4HSO_4) and ammonium sulfate ($(NH_4)_2SO_4$), depending on the extent of neutralization. Beyond ~80° W, the SO_4^{2-}:NH_4^+ molar ratio approached the full neutralization limit of 1:2 for $(NH_4)_2SO_4$, whereas near shore, SO_4^{2-}:NH_4^+ greatly exceeded 1:1 (that of NH_4HSO_4).

In the coarse mode, the anion:cation ratio averaged 1.03:1 away from shore, less acidic than in the fine mode. A coarse mode with pH less than 7 can be inferred from observations of chloride deficit, which are included in Fig. 9. Sulfuric and nitric acid vapors react with sea-salt aerosols that are initially rich in NaCl, forming HCl, which is vaporized to the atmosphere and results in increased acidity and reduced Cl^- in reacted sea-salt (e.g. Keene et al., 1990; McInnes et al., 1994). In the offshore region, a small Cl^- deficit of $-0.1\,\mu g\,m^{-3}$ was observed in the coarse mode. A greater deficit of $-0.9\,\mu g\,m^{-3}$ was seen near shore again because of pollution, as evidenced by the much higher submicron aerosol mass. With low aerosol calcium throughout the entire project ($0.1\,\mu g\,m^{-3}$), the less acidic coarse mode offshore than by the coast was due to the lower uptake of acidic species rather than a titration with alkaline dust materials.

We estimate the order of magnitude sea-salt oxidation rate of SO_2 in an analogous fashion to in-cloud oxidation (Eq. 10), but replace L_{WC} with the integrated supermicron

ACPD
11, 2873–2929, 2011

aerosol mass concentration derived from the *RHB* size distribution, which averaged $\sim 8\,\mu g\,m^{-3}$. At a pH of 6.0, the SO_2 reaction with O_3 is two orders of magnitude faster than the reaction with H_2O_2. With gas phase O_3 and SO_2 concentrations of 26 ppbv and 25 pptv, respectively, the instantaneous loss rate of $S(IV)$ due to O_3 is $\sim 1.2 \times 10^{-8}\,M\,s^{-1}$, implying a sea-salt SO_2 oxidation rate less than 0.01 pptv h^{-1}, negligible compared to other rates. At a pH of 6.5, the oxidation rate of SO_2 in sea-salt is increased to 0.08 pptv h^{-1}, but still less than half of the gas phase oxidation rate. By assuming the entire sea-salt volume was reactive and keeping the pH constant, the calculation above represents an upper level estimate because in real sea-salt aerosols, SO_4^{2-} production and uptake SO_2 by diffusion would acidify the aerosols eventually even with the carbonate buffer, further slowing the O_3 reaction. The insignificance of O_3 oxidation with regard to MBL SO_2 budget is consistent with the observation that only $5 \sim 6\%$ of the total non-sea-salt SO_4^{2-} was found in the coarse mode during VOCALS-REx per filter measurements. Moreover, this percentage was relatively insensitive to longitude, whereas the pH of sea-salt aerosols likely differed substantially from near shore to the remote marine region, suggesting that mechanisms other than O_3 oxidation (e.g. direct uptake of H_2SO_4, in-cloud oxidation by H_2O_2, and evaporation following wet scavenging) were responsible for SO_4^{2-} to be present in the coarse mode.

4.1.7 SO_2 budget summary

To more accurately calculate the sources and sinks of SO_2, we look at their time-evolutions over the course of a day and compare the implied SO_2 diurnal cycle with observations. From Eq. (2), omitting sea-salt oxidation, the column integrated concentration of SO_2 at time t can be written as:

$$\left\langle \overline{SO_2} \right\rangle_t = \left\langle \overline{SO_2} \right\rangle_{t-1} + (F_{SO_2,0})_{t-1} - (F_{SO_2,Z_i})_{t-1} + \left\langle P_{SO_2} \right\rangle_{t-1} - \left\langle L_{SO_2,OH} \right\rangle_{t-1} - \left\langle L_{SO_2,cloud} \right\rangle_{t-1} \quad (14)$$

ACPD
11, 2873–2929, 2011

The last five terms on the RHS represent time-integrated rates since the previous time step. C-130 Observations of SO_2 in the remote region were available in the hours of 08:00 ~ 20:00 UTC. We initialize our calculation with mean observation at 09:00 UTC (06:00 a.m. local) because that was approximately the time when the aircraft reached the westernmost location (80 ~ 85° W) on most 20° S survey flights. Compared to other hours, observations from 09:00 to 13:00 UTC should be subject to the least amount of bias because the aircraft usually stayed in the same general area. DMS and OH cycles are calculated as in Yang et al. (2009) for the remote region and used to estimate SO_2 production assuming conversion efficiencies of 0.7 and 0.9 from DMS to SO_2. Over 24 h, we consider the budget closed when the concentration at the end of the calculation matches that at the beginning under the assumptions of steady state and stationarity.

From direct measurements of DMS, O_3, and water vapor fluxes, Faloona et al. (2005) estimated higher ω_e at night in the stratocumulus region off the coast of California due to greater radiatively driven turbulence and cloud coverage than during the day, qualitatively consistent with findings from Bretherton et al. (2004) in the SEP. We can roughly approximate the diel variability in ω_e for VOCALS-REx by linearizing the mean $\omega_e = 4\,\mathrm{mm\,s^{-1}}$ with cloud fraction at each hour relative to the mean cloud fraction (0.67), which leads to $6\,\mathrm{mm\,s^{-1}}$ at night and $2\,\mathrm{mm\,s^{-1}}$ during the day. As seen in Fig. 13, entrainment, deposition, and gas phase OH oxidation are all minor losses of SO_2. In-cloud oxidation, the largest sink for SO_2, is estimated using a fixed H_2O_2 concentration of 0.9 ppbv and constant pH of 4.2 (i.e. an open system). The concentration of SO_2 below Z_i is adjusted from the implied time dependent MBL SO_2 concentration using the observed gradient from C-130 profiles. The aqueous concentration of $S(IV)$ is equilibrated with the cloud level SO_2. Instead of using L_{WC} from the C-130 and guessing the time parcels spend in clouds, we use the liquid water path (L_{WP}) determined from the ship, which accounted for both cloudy and clear air conditions. For $\gamma = 0.9$, we find that the in-cloud oxidation loss term needs to be multiplied by a factor of 0.43 to balance the diel budget of SO_2. This factor is necessary probably

ACPD
11, 2873–2929, 2011

because we assumed an open system and calculated in-cloud oxidation based on implied SO_2 concentration at cloud level, which is influenced by both the MBL and the FT. For the MBL budget of SO_2 concentration, only SO_2 originated from the MBL and lost in clouds should be included. For the case of lower γ, the in-cloud oxidation term needs to be further reduced. We see in Fig. 13 that the implied SO_2 cycle matches well with observations until 13:00 UTC (a few hours after sunrise). Comparison worsens for subsequent hours, likely in part due to the large spatial variability and bias of the C-130 observations as the aircraft was then often profiling or transiting.

4.2 Sulfate budget

From an island-based experiment in the Equatorial Pacific, where the cloud cover is much lower and the decoupling between the surface and Z_i even more pronounced than in the SEP, Huebert et al. (1996) measured a clear diurnal cycle in SO_4^{2-} aerosols. SO_4^{2-} built up slowly during the day and peaked near sunset, consistent with photochemical production from SO_2. Dilution due to entrainment was mostly responsible for the nighttime SO_4^{2-} decline. In contrast to this diel trend, SO_4^{2-} during VOCALS-REx was the lowest in the late afternoon, increased rapidly over the first several hours after sunset, then decreased steadily and leveled off over the rest of the diel cycle. As with SO_2, we first look at the magnitudes of the different terms in the SO_4^{2-} budget:

$$\frac{\partial \left\langle \overline{SO_4^{2-}} \right\rangle}{\partial t} = F_{SO_4^{2-},0,\mathrm{dry}} + F_{SO_4^{2-},0,\mathrm{wet}} - F_{SO_4^{2-},Z_i} + \left\langle P_{SO_4^{2-}} \right\rangle \quad (15)$$

The first three terms on the RHS are dry deposition to the surface, wet deposition due to precipitation, and entrainment at the inversion, respectively. The last term represent in situ production of SO_4^{2-} from SO_2.

ACPD
11, 2873–2929, 2011

4.2.1 SO_4^{2-} dry deposition

The surface flux of SO_4^{2-} is related to the concentration near the surface ($[SO_{4,0}^{2-}]$):

$$F_{SO_{4,0,dry}^{2-}} = -\int_0^\infty V_{aero}(D)[SO_{4,0}^{2-}(D)]dD \quad (16)$$

The deposition velocity of particles, V_{aero}, is a strong function of particle size (D). Coarse particles deposit orders of magnitude faster due to gravitational settling than accumulation mode particles. At less than 0.02 µg m^{-3} (~5 pptv), only ~5% of the total non-sea-salt SO_4^{2-} was found in the coarse mode in the offshore region per filter measurements. However, the enhanced V_{aero} at supermicron sizes suggests that dry deposition flux should still be considered. Lacking size distributed SO_4^{2-} observations, we rely on shipboard APS aerosol size distribution and coarse SO_4^{2-} mass from filter measurements.

We estimate V_{aero} using the model from Slinn and Slinn (1980), with wet diameters adjusted from 60% RH to the ambient RH according to the sea-salt growth curve (Howell et al., 2006). At the upper size cutoff of the APS (10 µm at 60% RH, or ~11 µm at ambient RH), V_{aero} peaks at ~0.2 cm s^{-1}. Integrating mass distributions over supermicron sizes yields a concentration that agrees well with coarse gravimetric mass from the filters (~8 µg m^{-3}), of which ~0.5% was non-sea-salt SO_4^{2-}. To approximate size resolved SO_4^{2-}, we apply this percentage uniformly to the supermicron mass distribution (i.e. assuming coarse SO_4^{2-} has the same relative distribution as sea-salt aerosols). Previous impactor measurements in the remote Pacific showed that most of the coarse SO_4^{2-} is present at 2 ~ 3 µm, or towards the smaller end of the supermicon spectrum (R. Simpson, personal communication, 2010), whereas the distribution of sea-salt tends to be broader. Allocating more SO_4^{2-} to the larger end of the supermicon spectrum, where the deposition velocity is much higher, could thus overestimate deposition flux.

ACPD
11, 2873–2929, 2011

Multiplying the approximated SO_4^{2-} distribution by V_{aero} and summing over super-micron sizes leads to a mean surface flux of merely ~0.002 μmoles m^{-2} day^{-1}. Even with a ten-fold higher V_{aero}, the resultant deposition flux would still be only ~10% of the SO_4^{2-} production rate from the gas phase oxidation of SO_2, and orders of magnitude lower than other terms in the SO_4^{2-} budget, consistent with the suggestion from Rodhe (1978) that the residence time of SO_4^{2-} is much longer than that of SO_2 with respect to dry deposition. This result is unsurprising because the vast majority of the SO_4^{2-} mass was found in the accumulation mode, where dry deposition is very slow.

4.2.2 SO_4^{2-} entrainment

The entrainment of SO_4^{2-} is calculated similarly to that of SO_2 (Eq. 4). From average C-130 profiles, with a SO_4^{2-} concentration below $Z_i \sim 40$,pptv less than above, entrainment diluted the MBL at a rate of 0.5(±0.3) μmole m^{-2} day^{-1}, or 0.4(±0.2) pptv h^{-1}. The 20 ~ 30 pptv of SO_4^{2-} observed at cloud level was biased towards clear sky, cloud outflow, and POC regions, thus not representative of the concentration below Z_i. As with SO_2, considering the mass flux of SO_4^{2-} at Z_i to be only proportional to the FT concentration (~40 pptv), entrainment added 0.5(±0.3) μmole m^{-2} day^{-1} of SO_4^{2-} to the MBL. Together with the mass flux of SO_2 of 0.3(±0.2) μmoles m^{-2} day^{-1}, the upper limit contribution of anthropogenic sulfur mass from the FT to the MBL was 0.8(±0.4) μmoles m^{-2} day^{-1}, or ~20% of the DMS sea-to-air flux.

4.2.3 SO_4^{2-} production

The in situ production rate of SO_4^{2-} includes losses of SO_2 in both the gas phase and aqueous phase:

$$\left\langle P_{SO_4^{2-}} \right\rangle = \left\langle P_{SO_4^{2-},OH} \right\rangle + \left\langle P_{SO_4^{2-},cloud} \right\rangle \quad (17)$$

ACPD
11, 2873–2929, 2011

To balance the SO_2 budget in the MBL (Eq. 12), excluding the fraction of SO_2 originated from the FT, 2.1 µmoles m^{-2} of SO_2 needs to be oxidized in clouds over the entire day. Considering the additional FT SO_2 contribution, 4.0 µmoles m^{-2} of SO_4^{2-} was produced in-cloud in 24 hours. This rate (equivalent to 78 pptv day^{-1}) is similar to what was reported by Huebert et al. (1996) and Clarke et al. (1996) over the Equatorial Pacific.

4.2.4 SO_4^{2-} wet deposition

Because of its high water solubility, SO_4^{2-} is readily taken up in clouds. Coalescence of cloud droplets form precipitation, which removes aerosols both scavenged in-cloud and collected in the column of air below while falling. Figure 14 shows SO_4^{2-} vs. rain rate reaching the surface (P_d) measured by the shipboard rain gauge, color-coded by longitude. The heaviest precipitation events (> 1 mm h^{-1}) occurred west of 80° W and were associated with the lowest SO_4^{2-}. The average P_d of 0.01 mm h^{-1} in the remote region (including non-precipitating periods) is consistent with the typical cloud base drizzle rate of $1 \sim 2$ mm day^{-1} derived from C-130 radar and lidar measurements, with $10 \sim 20$% reaching the surface (Bretherton et al. 2010).

The wet deposition flux of SO_4^{2-} is the sum of below cloud scavenging ($F_{SO_4^{2-},0,BC}$) and in-cloud scavenging ($F_{SO_4^{2-},0,IC}$). The below cloud scavenging rate of SO_4^{2-} by droplets reaching the surface depends on the mean MBL concentration:

$$F_{SO_4^{2-},0,BC} = -\Lambda_{BC}[SO_4^{2-}]H_{BC} \quad (18)$$

Here Λ_{BC} is the below cloud scavenging coefficient of SO_4^{2-}, which is a function of rain rate and the collection efficiency. Andronache (2003) showed that small drizzle droplets are more efficient at scavenging aerosols than larger rain droplets. Scavenging by falling droplets is particularly efficient for coarse particles (by impaction) and for nuclei mode particles (by Brownian motion). In contrast, accumulation size particles lie in the "scavenging well" and have the lowest efficiency. From Seinfeld and Pandis (2006),

ACPD
11, 2873–2929, 2011

for typical drizzle diameter of 0.2 mm and 200 ∼ 300 nm aerosols (mean diameter for SO_4^{2-} mass during VOCALS-REX), Λ_{BC} is about 0.01 h^{-1} for a rain rate of 1 mm h^{-1}. We estimate Λ_{BC} [h^{-1}] as 0.01 (P_d/1). For a well-mixed MBL, H_{BC} is the height from the surface to the bottom of a precipitating cloud, which we approximate with MLH. From Eq. (15), we calculate a below cloud SO_4^{2-} wet removal of 0.006 µmole m^{-2} day^{-1} on average and ∼0.1 µmole m^{-2} day^{-1} for heavy rain events.

Most of the wet removal of SO_4^{2-} was due to in-cloud scavenging. When cloud forms in a rising air parcel, SO_4^{2-} aerosols mostly become cloud droplets (nucleation scavenging) and are later removed by precipitation. ten Brink et al. (1986) found very low levels of aerosol SO_4^{2-} in cloud interstitial air compared to cloud-free air, suggesting a high scavenging efficiency at relatively low concentrations by cloud droplets. The in-cloud scavenging of SO_4^{2-} is formulated similarly to below cloud scavenging, but with in-cloud scavenging coefficient (Λ_{IC}) and concentration integrated to Z_i:

$$F_{SO_4^{2-},0,IC} = -\Lambda_{IC} \left\langle \overline{SO_4^{2-}} \right\rangle \tag{19}$$

Okita et al. (1996) found a bulk scavenging efficiency of 0.5 $P_d^{0.74}$ h^{-1} from SO_4^{2-} measurements over the Sea of Japan during a winter monsoon. Following theories from Scott (1982) and constrained by bulk precipitation measurements from the Eastern United States, Andronache (2004) parameterized Λ_{IC} of SO_4^{2-} using a Marshall and Palmer (1948) precipitation size distribution: 1.26 $P_d^{0.78}$ h^{-1}. Utilizing at the moment the parameterization from Okita et al. (1996), the in-cloud scavenging loss would be ∼1.2 µmole m^{-2} day^{-1} and over 25 µmole m^{-2} day^{-1} for the heaviest precipitation events.

ACPD
11, 2873–2929, 2011

4.2.5 SO_4^{2-} budget summary

Assuming a well-mixed MBL and omitting dry deposition, the column integrated concentration of SO_4^{2-} at time t can be written as:

$$\left\langle \overline{SO_4^{2-}} \right\rangle_t = \left\langle \overline{SO_4^{2-}} \right\rangle_{t-1} - (F_{SO_4^{2-},Z_i})_{t-1} + \left\langle P_{SO_4^{2-}} \right\rangle_{t-1} - \left\langle L_{SO_4^{2-},wet} \right\rangle_{t-1} \quad (20)$$

Shipboard SO_4^{2-} measurements were taken in the remote region during 24 ~ 30 October and 16 ~ 17 November. We initiate our calculation with the observation at 00:00 UTC and compute over one diel cycle. To quantify the average effect of episodic rainfall, the mean precipitation rate of 0.01 mm h^{-1} is linearized with the relative cloud fraction, as done with ω_e. We found that Λ_{IC} of 1.0 $P_d^{0.74}$ h^{-1}, which is between the parameterizations from Okita et al. (1996) and Andronache (2004), results in a general budget balance. As seen in Fig. 15, being proportional to L_{WC}, the in-cloud oxidation of SO_2 peaks in the early morning, which is largely offset by wet deposition that also peaks at the same time when cloud fraction was usually the highest. Without clouds, gas phase oxidation would slowly build up SO_4^{2-} during the day, as in Huebert et al. (1996). However, the processes above do not capture the observed diel trend in VOCALS-REx.

That the surface O_3 concentration (which had a FT source) increased along with SO_4^{2-} in the early evening suggests that the main source of SO_4^{2-} spike was from above. High levels of SO_4^{2-} were not usually observed in the remote FT, which left the upper MBL to be the more likely source, with SO_4^{2-} produced in clouds. During the day, due to the decoupling of the MBL, SO_4^{2-} generated in clouds could be isolated in the upper MBL. The recoupling of the MBL after sunset would mix down this air rich in SO_4^{2-}, causing a spike in measured concentration. SO_4^{2-} was then depleted by wet deposition over the rest of diurnal cycle, with the most rapid loss in the early morning. To test this proposed mechanism, instead of adding in-cloud SO_2 oxidation to the SO_4^{2-} budget

ACPD
11, 2873–2929, 2011

continuously as in Eq. (17), we sum in-cloud SO_2 oxidation over 24 h and incorporate it to MBL SO_4^{2-} budget only during the first four hours after sunset. The daily production of SO_4^{2-} in cloud amounted to 4.0 µmoles m^{-2}, similar to the increase observed from 00:00 to 04:00 UTC. Thus we add 1.0 µmole m^{-2} of SO_4^{2-} to each of these four hours and recalculate the SO_4^{2-} budget (Fig. 16). As wet depositional loss is first order, the large amount of SO_4^{2-} added initially is adequately depleted over the rest of the diurnal cycle and the implied diel variability is qualitatively similar to observations.

The major rates in the MBL SO_2 and SO_4^{2-} budgets are shown in Table 1, with both choices of γ. A refinement to the one layer box model utilized here for our diel calculations would be to solve the upper and lower parts of the MBL separately in the decoupled daytime; at night the two layers would join to become one. However, not knowing the exchange between the upper and lower parts of the MBL during the day makes the implementation of such a dynamical model difficult for the time being.

5 Conclusions

In order to evaluate the effects of anthropogenic sulfur inputs to the atmosphere, we must first understand the natural background cycles. In VOCALS-REx, multi-platform observations and relatively simple dynamics of the stratocumulus capped marine boundary layer allowed us estimate the sources and sinks of DMS, SO_2, and SO_4^{2-} aerosols. The sea-to-air flux of DMS (3.8 ± 0.4 µmoles m^{-2} day^{-1}), rather than "mass" entrainment of SO_2 and SO_4^{2-} (0.8 ± 0.4 µmoles m^{-2} day^{-1}), was the predominant source of sulfur mass to the remote region of the SEP. Accounting for dilution due to entrainment (0.7 ± 0.3 µmoles m^{-2} day^{-1}), the remaining DMS was oxidized by OH to mostly SO_2. The SO_2 production rate from DMS was calculated to be $2.2 \sim 2.8$ µmoles m^{-2} day^{-1} using a DMS to SO_2 conversion efficiency of $0.7 \sim 0.9$, peaking at $7.5 \sim 9.7$ µmoles m^{-2} day^{-1} in midday. From our implied diel cycle calculations ($\gamma = 0.9$), entrainment slightly increased the MBL SO_2 burden

ACPD
11, 2873–2929, 2011

at a rate of $0.05 \pm 0.02\,\mu moles\,m^{-2}\,day^{-1}$, while dry deposition decreased SO_2 at a rate of $0.6 \pm 0.1\,\mu moles\,m^{-2}\,day^{-1}$. The gas phase oxidation of SO_2 was about $0.2\,\mu moles\,m^{-2}\,day^{-1}$ on a diel average, peaking at $0.9\,\mu moles\,m^{-2}\,day^{-1}$ in the afternoon. The largest SO_2 loss term was in-cloud oxidation to SO_4^{2-} at approximately $2.1 \pm 0.5\,\mu moles\,m^{-2}\,day^{-1}$, which appears to balance the SO_2 budget and suggests other potential removal mechanisms were insignificant. With a slightly acidic coarse mode, our order of magnitude estimations of SO_2 oxidation by O_3 in sea-salt aerosols using measured size distribution yielded negligible rates. Entrainment diluted SO_4^{2-} burden at a rate of $0.5 \pm 0.3\,\mu moles\,m^{-2}\,day^{-1}$, while dry deposition represented an insignificant sink for SO_4^{2-} because little non-sea-salt SO_4^{2-} mass was present in the coarse mode.

Diurnally, the implied SO_2 cycle shows a maximum in concentration near sunset due to oxidation of DMS by OH and minimum just after sunrise as a result of in-cloud oxidation, with dry deposition being a continuous loss term. This diel pattern is anticorrelated with that of DMS, consistent with previous observations in the remote Pacific. The SO_4^{2-} diel cycle observed on the ship appeared to be related to boundary layer dynamics and the intricately connected in-cloud production and wet removal. SO_4^{2-} produced in cloud was confined to near cloud level during the day, when the upper and lower parts of the MBL were usually decoupled. As the MBL recoupled after nightfall, the large amount of SO_4^{2-} built up at cloud level was mixed downwards, increasing the concentration at the surface. After peaking in the middle of the night, SO_4^{2-} steadily declined and leveled off for the rest of the day mostly as a result of decoupling and wet removal by precipitation.

ACPD
11, 2873–2929, 2011

Acknowledgements. We thank the National Science Foundation for support of this work through grant ATM-0241611, ATM-0526341, ATM-0744636, and ATM-0745337. Aircraft thermodynamic data and ancillary gas concentrations were provided by NCAR/EOL under sponsorship of the NSF (http://data.eol.ucar.edu/master_list/?project=VOCALS). PMEL data were downloaded from http://saga.pmel.noaa.gov/data/download.php?cruise=VOCALS. Special thanks to R. A. Weller, C. W. Fairall, R. Wood, C. S. Bretherton, R. M. Simpson, as well as the crews of *RHB* and C-130.

References

Andronache, C.: Estimated variability of below-cloud aerosol removal by rainfall for observed aerosol size distributions, Atmos. Chem. Phys., 3, 131–143, doi:10.5194/acp-3-131-2003, 2003.

Andronache, C.: Estimates of sulfate aerosol wet scavenging coefficient for locations in the Eastern United States, Atmos. Environ., 38(6), 795–804, doi:10.1016/j.atmosenv.2003.10.035, 2004.

Bandy, A. R., Thornton, D. C., Blomquist, B. W., Chen, S., Wade, T. P., Ianni, J. C., Mitchell, G. M., and Nadler W.: Chemistry of dimethyl sulfide in the equatorial Pacific atmosphere, Geophys. Res. Lett., 23(7), 741–744, doi:10.1029/96GL00779, 1996.

Bandy, A. R., Thornton, D. C., Tu, F. H., Blomquist, B. W., Nadler, W., Mitchell, G. M., and Lenchow D. H.: Determination of the vertical flux of dimethylsulfide by eddy correlation and atmospheric pressure ionization mass spectrometry (APIMS), J. Geophys. Res., 107(D24), 4743, doi:10.1029/2002JD002472, 2002.

Bates, T. S., Calhoun, J. A., and Quinn, P. K.: Variations in the Methanesulfonate to Sulfate Molar Ratio in Submicrometer Marine Aerosol Particles Over the South Pacific Ocean, J. Geophys. Res., 97(D9), 9859–9865, doi:10.1029/92JD00411, 1992.

Bates, T. S., Quinn, P. K., Covert, D. S., Coffman, D. J., Johnson, J. E., and Wiedensohler, A.: Aerosol physical properties and processes in the lower marine boundary layer: A comparison of shipboard sub-micron data from ACE-1 and ACE-2, Tellus B, 52, 258–272, 2000.

Bates, T. S., Quinn, P. K., Coffman, D., Schulz, K., Covert, D. S., Johnson, J. E., Williams, E. J., Lerner, B. M., Angevine, W. M., Tucker, S. C., Brewer, W. A., and Stohl, A.: Boundary layer aerosol chemistry during TexAQS/GoMACCS 2006: Insights into aerosol sources

ACPD

11, 2873–2929, 2011

and transformation processes, J. Geophys. Res., 113, D00F01, doi:10.1029/2008JD010023, 2008.
Bretherton, C. S., Uttal, T., Fairall, C. W., Yuter, S. E., Weller, R. A., Baumgardner, D., Comstock, K., Wood, R., and Rag, G. B.: The EPIC 2001 stratocumulus study, B. Am. Meteorol. Soc., 85(7), 967–977, 2004.
Bretherton, C. S., Wood, R., George, R. C., Leon, D., Allen, G., and Zheng, X.: Southeast Pacific stratocumulus clouds, precipitation and boundary layer structure sampled along 20° S during VOCALS-REx, Atmos. Chem. Phys. Discuss., 10, 15921–15962, doi:10.5194/acpd-10-15921-2010, 2010.
Blomquist, B. W., Huebert, B. J., Fairall, C. W., and Faloona, I. C.: Determining the sea-air flux of dimethylsulfide by eddy correlation using mass spectrometry, Atmos. Meas. Tech., 3, 1–20, doi:10.5194/amt-3-1-2010, 2010.
Caldwell, P., Bretherton, C. S., and Wood, R.: Mixed-Layer Budget Analysis of the Diurnal Cycle of Entrainment in Southeast Pacific Stratocumulus, J. Atmos. Sci., 62(10), 3775–3791, 2005.
Chameides, W. L.: The photochemistry of a remote marine stratiform cloud, J. Geophys. Res., 89(D3), 4739–4755, doi:10.1029/JD089iD03p04739, 1984.
Charlson, R. J., Lovelock, J. E., Andreae, M. O., and Warren S. G.: Oceanic phytoplankton, atmospheric sulfur, cloud albedo and climate, Nature, 326, 655–661, 1987.
Charlson, R. J., Schwartz, S. E., Hales, J. M., Cess, R. D., Coakley Jr., J. A. , Hansen, J. E., and Hoffman, D. J.: Climate forcing by anthropogenic aerosols, Science, 255, 423–3430, 1992.
Clarke, A. D., Li, Z., and Litchy, M.:Aerosol dynamics in the equatorial Pacific marine boundary layer: Microphysics, diurnal cycles and entrainment, Geophys. Res. Lett., 23(7), 733–736, doi:10.1029/96GL00778, 1996.
Clarke, A. D., Davis, D., Kapustin, V. N., Eisele, F., Chen, G., Paluch, I., Lenschow, D., Bandy, A. R., Thornton, D., Moore, K., Mauldin, L., Tanner, D., Litchy, M., Carroll, M. A., Collins, J., and Albercook, G.: Particle nucleation in the tropical boundary layer and its coupling to marine sulfur sources. Science, 282, 89–92, 1998.
de Szoeke, S. P., Fairall, C. W., and Pezoa, S.: Ship Observations of the Tropical Pacific Ocean along the Coast of South America, J. Climate, 22, 458–464, 2008.
Fairall, C. W., Helmig, D., Ganzeveld, L., and Hare, J.: Water-side turbulence enhancement of ozone deposition to the ocean, Atmos. Chem. Phys., 7, 443–451, doi:10.5194/acp-7-443-2007, 2007.

ACPD
11, 2873–2929, 2011

Faloona, I.: Sulfur processing in the marine atmospheric boundary layer: A review and critical assessment of modeling uncertainties, Atmos. Environ., 43(18), 2841–2854, doi:10.1016/j.atmosenv.2009.02.043 2009.

Faloona, I., Conley, S., Blomquist, B., Clarke, A., Kapustin, V., Howell, S., Lenschow, D. H., and Bandy, A.: Sulfur dioxide in the tropical marine boundary layer: dry deposition and heterogeneous oxidation observed during the Pacific Atmospheric Sulfur Experiment, J. Atmos. Chem., 63(1), 13–32, doi:10.1007/s10874-010-9155-0, 2010.

Faloona, I., Lenschow, D., Campos, T., Stevens, B., van Zanten, M., Blomquist, B., Thornton, D., Bandy, A., and Gerber, H.: Observations of Entrainment in Eastern Pacific Marine Stratocumulus Using Three Conserved Scalars, J. Atmos. Sci., 62, 3268–3285, 2005.

Feingold, G., Kreidenweis, S., and Zhang, Y.: Stratocumulus processing of gases and cloud condensation nuclei 1. Trajectory ensemble model, J. Geophys. Res., 103(D16), 19527–19542, 1998.

Hawkins, L. N., Russell, L. M., Covert, D. S., Quinn, P. K., and Bates T. S.: Carboxylic acids, sulfates, and organosulfates in processed continental organic aerosol over the southeast Pacific Ocean during VOCALS-REx 2008, J. Geophys. Res., 115, D13201, doi:10.1029/2009JD013276, 2010.

Hegg, D. A.: The importance of liquid-phase oxidation of SO_2 in the troposphere, J. Geophys. Res., 20, 3773–377, 1985.

Hoffmann, M. R. and Calvert, J. G.: Chemical transformation modules for Eulerian acid deposition models, Volume 2, The Aqueous-Phase Chemistry, EPA/600/3-85/017, US Environmental Protection Agency, Research Triangle Park, NC, 1985.

Hoppel, W. A., Frick, G. M., and Larson, R. E.: Effect of nonprecipitating clouds on the aerosol size distribution in the marine boundary layer, Geophys. Res. Lett., 13(2), 125–128, doi:10.1029/GL013i002p00125, 1986.

Howell, S. G., Clarke, A. D., Shinozuka, Y., Kapustin, V., McNaughton, C. S., Huebert, B. J., Doherty, S. J., and Anderson, T. L.: Influence of relative humidity upon pollution and dust during ace-Asia: Size distributions and implications for optical properties, J. Geophys. Res. Atmos. 111(D6), D06205, doi:10.1029/2004JD005759, 2006.

Huebert, B. J., Wylie, D. J., Zhuang, L., and Heath, J. A.: Production and loss of methanesulfonate and non-sea salt sulfate in the equatorial Pacific marine boundary layer, Geophys. Res. Lett., 23, 737–740, 1996.

Huebert, B., Blomquist, B., Hare, J., Fairall, C., Johnson, J., and Bates, T.: Measurement of

ACPD
11, 2873–2929, 2011

the sea-air DMS flux and transfer velocity using eddy correlation, Geophys. Res. Lett., 31, L23113, doi:10.1029/2004GL021567, 2004.
Huebert, B. J., Howell, S. G., Covert, D., Bertram, T., Clarke, A., Anderson, J. R., Lafleur, B. G., Seebaugh, W. R., Wilson, J. C., Gesler, D., Blomquist, B., and Fox, J: PELTI: Measuring the Passing Efficiency of an Airborne Low Turbulence Aerosol Inlet, Aerosol Sci. Technol., 38, 803–826, 2004.
Keene, W. C., Pszenny, A. A. P., Jacob, D. J., Duce, R. A., Galloway, J. N., Schultz-Tokos, J. J., Sievering, H., and Boatman, J. F.: The geochemical cycling of reactive chlorine through the marine troposphere, Global Biogeochem. Cy., 4, 407–430, 1990.
Kettle, A. J. and Andreae, M. O.: Flux of dimethylsulfide from the oceans: a comparison of updated data sets and flux models, J. Geophys. Res., 105(D22), 26793–26808, doi:10.1029/2000JD900252, 2000.
Lee, G., Park, J., Jang, Y., Lee, M., Kim, K., Oh, R., Kim, D., Yi, H., and Kim, T.: Vertical variability of seawater DMS in the South Pacific Ocean and its implication for atmospheric and surface seawater DMS, Chemosphere, 78(8), 1063–1070, doi:10.1016/j.chemosphere.2009.10.054, 2010.
Lilly, D. K.: Models of cloud-topped mixed layers under a strong inversion. Q. J. Roy. Meteorol. Soc., 94, 292–309, 1968.
Maahs, H. G.: Sulfur dioxide/water equilibrium between 0° and 50°: An examination of data at low concentrations, in: Heterogeneous Atmospheric Chemistry, edited by: Schryer, D. R., 187–195, AGU, Washington, DC, 1983.
Marshall, J. S. and Palmer, W. M.: The distribution of raindrop with size, J. Meteorol., 5, 165–166, 1948.
Martin, L. and Damschen, D. E.: Aqueous oxidation of sulfur dioxide by hydrogen peroxide at low pH, Atmos. Environ., 15(9), 1615–1621, doi:10.1016/0004-6981(81)90146-3, 1981.
McInnes, L. M., Covert, D. S., Quinn, P. K., and Germani, M. S.: Measurements of chloride depletion and sulfur enrichment in individual sea-salt particles collected from the remote marine boundary-layer, J. Geophys. Res., 99(D4), 8257–8268, doi:10.1029/93JD03453, 1994.
Nicholls, S.: The dynamics of stratocumulus: aircraft observations and comparisons with a mixed layer model, Q. J. Roy. Meteorol. Soc., 110, 783–820, 1984.
Okita, T., Hara, H., and Norio F.: Measurements of atmospheric SO_2 and SO_4^{2-}, and determination of the wet scavenging coefficient of sulfate aerosols for the winter monsoon season over the sea of Japan, Atmos. Environ., 30(22), 3733–3739, doi:10.1016/1352-2310(96)00090-8,

ACPD
11, 2873–2929, 2011

1996.
Perry, K. D. and Hobbs, P. V.: Further evidence for particle nucleation in clear air adjacent to marine cumulus clouds, J. Geophys. Res., 99(D11), 22803–22818, doi:10.1029/94JD01926, 1994.
Rahn, D. A. and Garreaud, R.: Marine boundary layer over the subtropical southeast Pacific during VOCALS-REx - Part 2: Synoptic variability, Atmos. Chem. Phys., 10, 4507–4519, doi:10.5194/acp-10-4507-2010, 2010.
Rodhe, H.: Budgets and turn-overtimes of atmospheric sulfur compounds, Atmos. Environ., 12, 671–680, 1978.
Sander, S. P., Golden, D. M., Kurylo, M. J., Moortgat, G. K., Wine, P. H., Ravishankara, A. R., Kolb, C. E., Molina, M. J., Finlayson-Pitts, B. J., Huie, R. E., and Orkin, V. L.: Chemical Kinetics and Photochemical Data for Use in Atmospheric Studies, Evaluation Number 15, Jet Propulsion Laboratory, Pasadena, CA, available at: http://jpldataeval.jpl.nasa.gov/, 2006.
Schwartz, S. E.: Mass transport limitation to the rate of in-cloud oxidation of SO_2: reexamination in the light of new data, Atmos. Environ., 22, 2491–2499, 1988.
Scott, B. C.: Theoretical estimates of the scavenging coefficient for soluble aerosol particles as a function of precipitation type, rate and altitude, Atmos. Environ., 16, 1753–1762, 1982.
Seinfeld, J. H. and Pandis, S. N.: Atmospheric chemistry and physics: from air pollution to climate change, 2nd ed. Wiley-Interscience. Hoboken, New Jersey, USA, 2006.
Sievering, H., Cainey, J., Harvey, M., McGregor, J. Nichol, S., and Quinn, P.: Aerosol non-sea-salt sulfate in the remote marine boundary layer under clear-sky and normal cloudiness conditions: Ocean-derived biogenic alkalinity enhances sea-salt sulfate production by ozone oxidation, J. Geophys. Res., 109, D19317, doi:10.1029/2003JD004315, 2004.
Slinn, S. A. and Slinn, W. G. N.: Predictions for particle deposition on natural waters, Atmos. Environ., 14, 1013–1016, 1980.
Stevens, B., Vali, G., Comstock, K., Wood, R., VanZanten, M., Austin, P. H., Bretherton, C. S., and Lenschow, D. H.: Pockets of Open Cells (POCs) and Drizzle in Marine Stratocumulus, B. Am. Meteorol. Soc., 86, 51–57, 2005.
Straub, D. J. and Collett, J. L:, An axial-flow cyclone for aircraft-based cloud water sampling, J. Atmos. Ocean. Tech., 21(12), 1825–1839, 2004.
Straub, D. J., Lee, T., and Collett Jr. J. L.: Chemical composition of marine stratocumulus clouds over the eastern Pacific Ocean, J. Geophys. Res., 112, D04307, doi:10.1029/2006JD007439, 2007.

ACPD
11, 2873–2929, 2011

Ten Brink, H. M., Schwartz, S. E., and Daum, P. H.: Efficient scavenging of aerosol sulfate by liquid-water clouds, Atmos. Environ., 21(9), 2035–2052, doi:10.1016/0004-6981(87)90164-8, 1986.

Thornton, D. C., Bandy, A. R., Tu, F. H., Blomquist, B. W., Mitchell, G. M., Nadler, W., and Lenschow, D. H.: Fast airborne sulfur dioxide measurements by atmospheric pressure ionization mass spectrometry (APIMS), J. Geophys. Res. Atmos., 107(D22), 4632, doi:10.1029/2002JD002289, 2002.

Tucker, S., Senff, C. J., Weickmann, A. M., Brewer, W. A., Banta, R. M., Sandberg, S. P., Law, D. C., Hardesty, R. M.: Doppler Lidar Estimation of Mixing Height Using Turbulence, Shear, and Aerosol Profiles, J. Atmos. Ocean. Tech., 26, 673–688. 2009.

Twomey, S.: Aerosols, clouds and radiation, Atmos. Environ., 25(11), 2435–2442, 1991.

Wesely, M. L. and Hicks B. B.: Some factors that affect deposition rates of sulfur-dioxide and similar gases on vegetation, J. Air Pollut. Control Assoc., 27(11), 1110–1116, 1977.

Wood, R. and Bretherton, C. S.: Boundary Layer Depth, Entrainment, and Decoupling in the Cloud-Capped Subtropical and Tropical Marine Boundary Layer, J. Climate, 17, 3576–3588, 2004.

Wood, R., Mechoso, C. R., Bretherton, C. S., Weller, R. A., Huebert, B., Straneo, F., Albrecht, B. A., Coe, H., Allen, G., Vaughan, G., Daum, P., Fairall, C., Chand, D., Gallardo Klenner, L., Garreaud, R., Grados, C., Covert, D. S., Bates, T. S., Krejci, R., Russell, L. M., de Szoeke, S., Brewer, A., Yuter, S. E., Springston, S. R., Chaigneau, A., Toniazzo, T., Minnis, P., Palikonda, R., Abel, S. J., Brown, W. O. J., Williams, S., Fochesatto, J., Brioude, J., and Bower, K. N.: The VAMOS Ocean-Cloud-Atmosphere-Land Study Regional Experiment (VOCALS-REx): goals, platforms, and field operations, Atmos. Chem. Phys., 11, 627–654, doi:10.5194/acp-11-627-2011, 2011.

Yang, M., Blomquist, B., Fairall, C., Archer, S., and Huebert, B.: Air-sea Exchange of Dimethylsulfide (DMS) in the Southern Ocean – Measurements from SO GasEx Compared to Temperate and Tropical Regions, J. Geophys. Res., in revision, 2011.

Yang, M., Blomquist, B. W., and Huebert, B. J.: Constraining the concentration of the hydroxyl radical in a stratocumulus-topped marine boundary layer from sea-to-air eddy covariance flux measurements of dimethylsulfide, Atmos. Chem. Phys., 9, 9225–9236, doi:10.5194/acp-9-9225-2009, 2009.

Yin, F., Grosjean, D., and Seinfeld, J.: Photooxidation of dimethylsulfide and dimethyldisulfide, I, Mechanism development, J. Atmos. Chem., 11, 309–364, 1990.

ACPD
11, 2873–2929, 2011

Zhang, Y., Kreidenweis, S., and Feingold G.: Stratocumulus processing of gases and cloud condensation nuclei 2. Chemistry sensitivity analysis, J. Geophys. Res., 104(D13), 16061–16080 1999.

Zhuang, L. and Huebert, B. J.: Lagrangian analysis of the total ammonia budget during Atlantic Stratocumulus Transition Experiment/Marine Aerosol and Gas Exchange, J. Geophys. Res., 101(D2), 4341–4350, doi:10.1029/95JD02467, 1996.

Zuidema, P., Westwater, E., Fairall C., and Hazen, D.: Ship-based Liquid Water Path Estimates in Marine Stratocumulus, J. Geophys. Res., 110, D20206, doi:10.1029/2005JD005833, 2005.

ACPD

11, 2873–2929, 2011

Table 1. Diel averaged rates in MBL concentration budgets of DMS, SO_2, and SO_4^{2-}.

DMS	µmole m^{-2} day^{-1}	pptv h^{-1}	% day^{-1}			
Sea-to-air Flux	3.81 ± 0.38	3.09 ± 0.31	118 ± 12			
Entrainment	−0.66 ± 0.33	−0.54 ± 0.27	−20 ± 10			
Loss to OH	−3.15 ± 0.50	−2.56 ± 0.41	−97 ± 16			
	$\gamma = 0.9$			$\gamma = 0.7$		
SO_2	µmole m^{-2} day^{-1}	pptv h^{-1}	% day^{-1}	µmole m^{-2} day^{-1}	pptv h^{-1}	% day^{-1}
Prod. from DMS	2.84 ± 0.45	2.30 ± 0.37	158 ± 25	2.21 ± 0.35	1.79 ± 0.29	134 ± 21
Entrainment	0.05 ± 0.02	0.04 ± 0.02	3 ± 1	0.06 ± 0.03	0.05 ± 0.03	4 ± 2
Dry Deposition	−0.56 ± 0.14	−0.45 ± 0.11	−31 ± 8	−0.51 ± 0.13	−0.41 ± 0.10	−31 ± 8
Loss to OH	−0.22 ± 0.03	−0.18 ± 0.02	−12 ± 2	−0.20 ± 0.03	−0.16 ± 0.02	−12 ± 2
Loss to Clouds	−2.10 ± 0.48	−1.70 ± 0.39	−117 ± 26	−1.56 ± 0.38	−1.27 ± 0.31	−95 ± 23
SO_4^{2-}	µmole m^{-2} day^{-1}	pptv h^{-1}	% day^{-1}	µmole m^{-2} day^{-1}	pptv h^{-1}	% day^{-1}
Prod. from SO_2	4.02 ± 0.89	3.26 ± 0.72	75 ± 16	3.32 ± 0.70	2.70 ± 0.57	62 ± 13
Entrainment	−0.51 ± 0.26	−0.41 ± 0.21	−9 ± 5	−0.28 ± 0.14	−0.23 ± 0.11	−5 ± 3
Wet Deposition	−3.51 ± 0.92	−2.85 ± 0.75	−65 ± 17	−3.04 ± 0.72	−2.47 ± 0.58	−56 ± 13

Positive (negative) indicate increases (decreases) in MBL concentrations. SO_2 and SO_4^{2-} rates are calculated with two separate DMS to SO_2 conversion efficiencies, 0.9 and 0.7. Percent daily rates are calculated with respect to observed (DMS and SO_4^{2-}) or implied (SO_2) daily mean concentrations. Errors for entrainment, dry deposition, and SO_2 oxidation are estimated from uncertainty in ω_e, V_{dep}, and [OH], with errors for other rates propagated under 95% confidence.

ACPD
11, 2873–2929, 2011

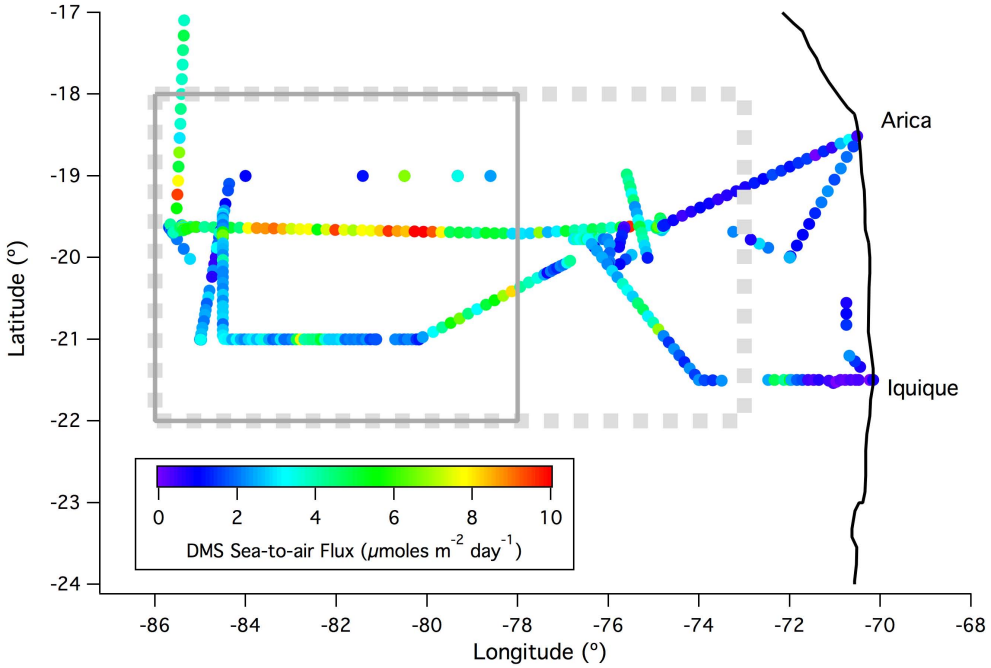

Fig. 1. VOCALS-REx cruise track color-coded by the DMS sea-to-air flux, which was higher offshore mostly as a result of higher wind speed. The dotted and solid boxes indicate the VOCALS "offshore" and "remote" regions, respectively.

ACPD
11, 2873–2929, 2011

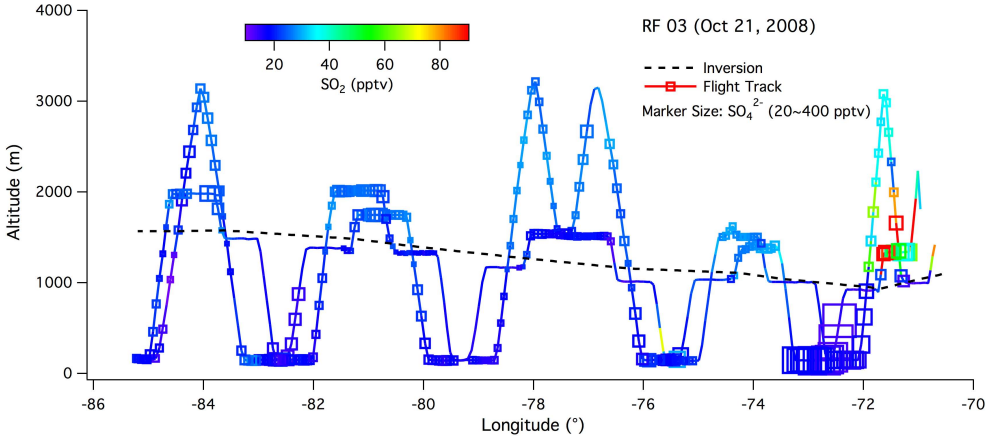

Fig. 2. A typical 20° S Survey flight by the C-130 (RF 03), with color indicating SO_2 concentration and marker size representing aerosol SO_4^{2-} concentration, with both sulfur species showing higher concentrations near shore than offshore. Level legs were typically flown near the surface, below the stratocumulus cloud deck, and above cloud, with occasional profiles to higher altitudes. Also included is the inversion height derived from C-130 profiles, which increased with distance away from shore.

ACPD
11, 2873–2929, 2011

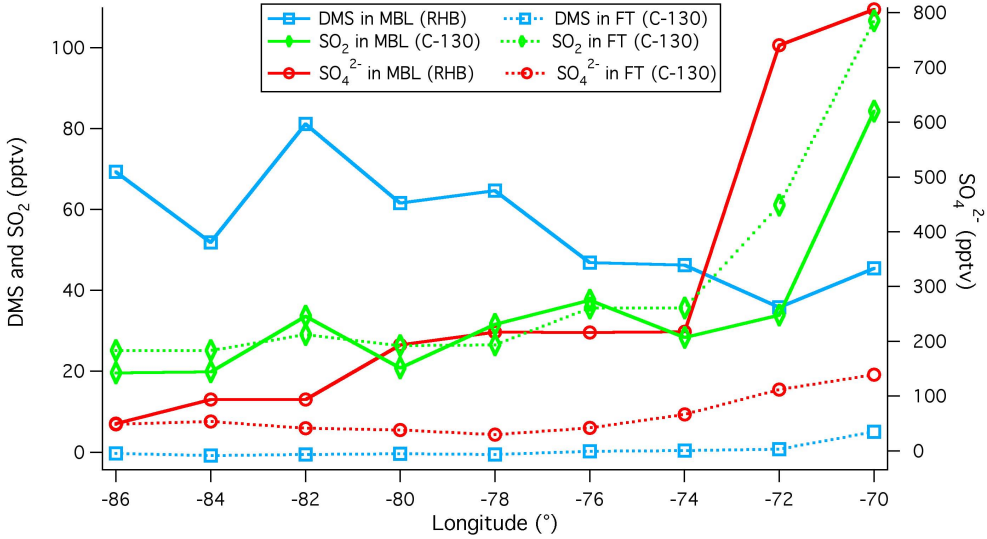

Fig. 3. Longitudinal trends in the atmospheric concentrations of DMS, SO_2, and SO_4^{2-} along 20(±2)° S in the MBL and FT (project means). SO_2 and SO_4^{2-} were significantly elevated near shore due to pollution, and rapidly decreased away from shore, where DMS was higher. In the remote atmosphere, the sea-to-air DMS flux accounted for about three quarters of the MBL sulfur burden, with the rest due to the entrainment of SO_2 and SO_4^{2-}.

ACPD
11, 2873–2929, 2011

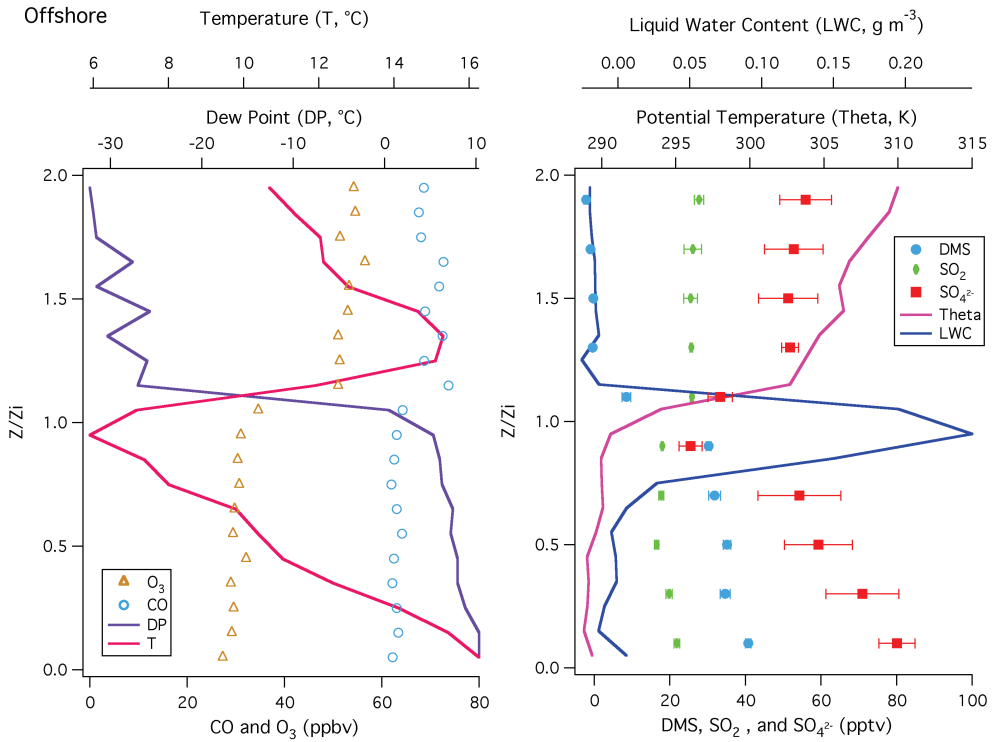

Fig. 4. (Left) averaged vertical profiles of temperature, dew point, CO, and O_3; (right) DMS, SO_2, SO_4^{2-} (with standard error of the mean), potential temperature, and liquid water content in the offshore region before sunrise. CO and O_3 concentrations were consistently greater above the sharp inversion ($Z/Z_i = 1$), while SO_4^{2-} was greater below the inversion.

ACPD
11, 2873–2929, 2011

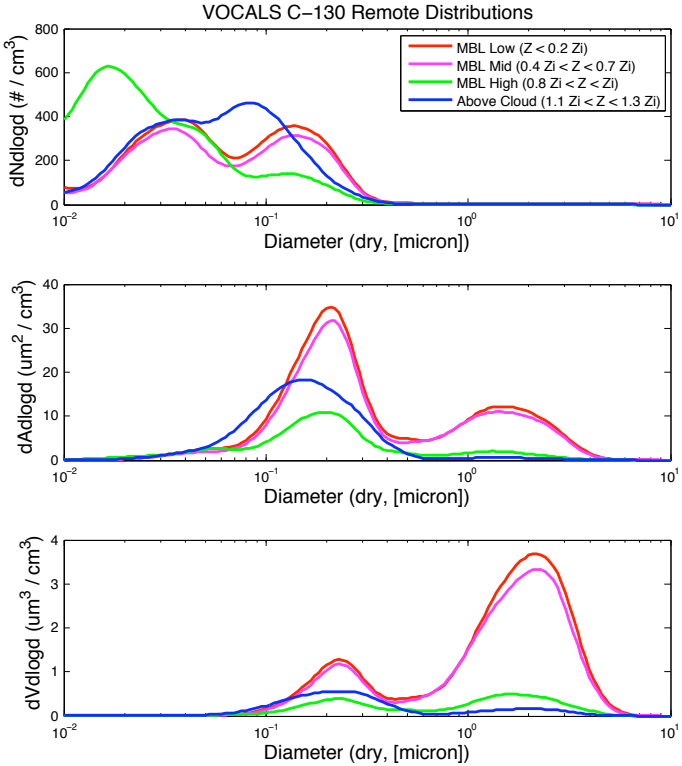

Fig. 5. Mean VOCALS C-130 remote particle number (top), surface area (middle), and volume distributions (bottom) at different normalized altitudes. The upper MBL distribution was reduced compared to lower and mid-MBL distributions, likely as a result of cloud scavenging and MBL decoupling. The above cloud distribution was a superposition of two modes, with the ~30 nm mode corresponding to low CO and the ~80 nm mode corresponding to high CO.

ACPD
11, 2873–2929, 2011

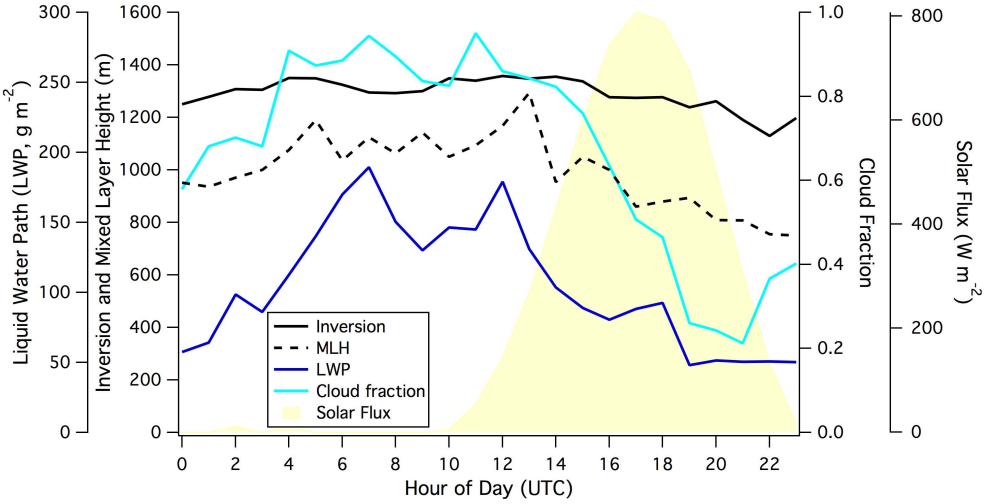

Fig. 6. Diel cycles in inversion height, mixed layer height, liquid water path, and cloud fraction in the VOCALS offshore region. All of these variables were greater at night than during the day mostly due to the diel variability in the radiative properties associated with the stratocumulus cloud deck.

ACPD
11, 2873–2929, 2011

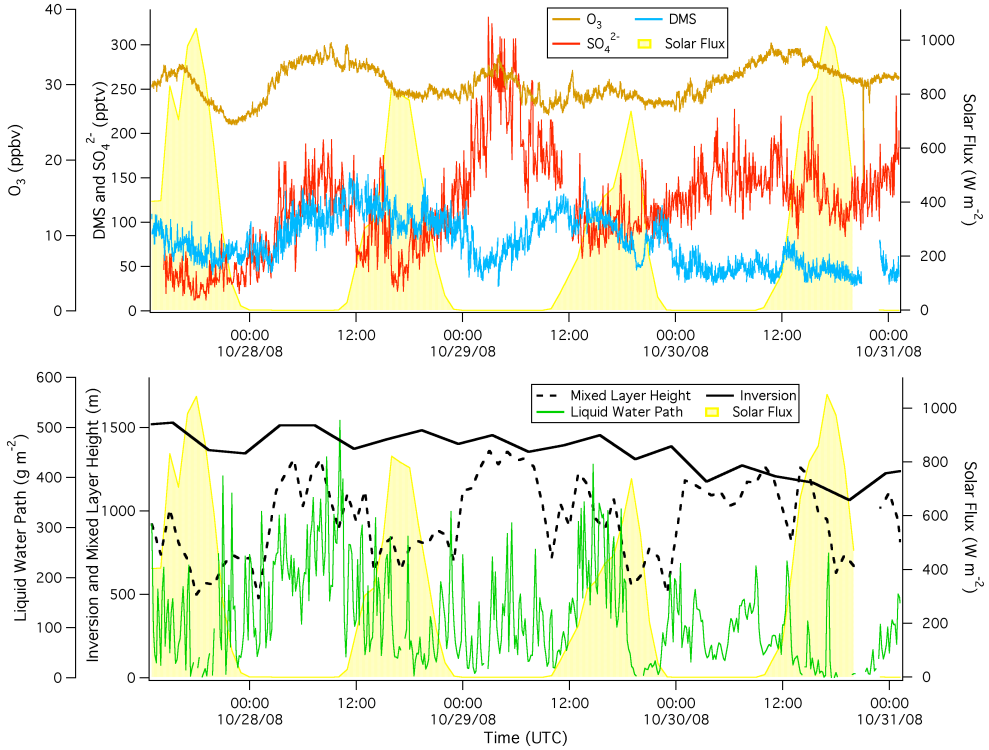

Fig. 7. Top panel: concentrations of O_3, DMS, and SO_4^{2-} from 28 ~ 31 October; bottom panel: liquid water path, mixed layer height, and inversion height for the same period. SO_4^{2-} frequently decreased during the day and peaked at night, as did O_3. MLH approached Z_i at night, suggesting a well-mixed MBL, whereas during the day MLH was only ~1/2 of Z_i, indicating decoupling. The nighttime increase in SO_4^{2-} was likely due to MBL coupling and in-cloud production of SO_4^{2-}.

ACPD
11, 2873–2929, 2011

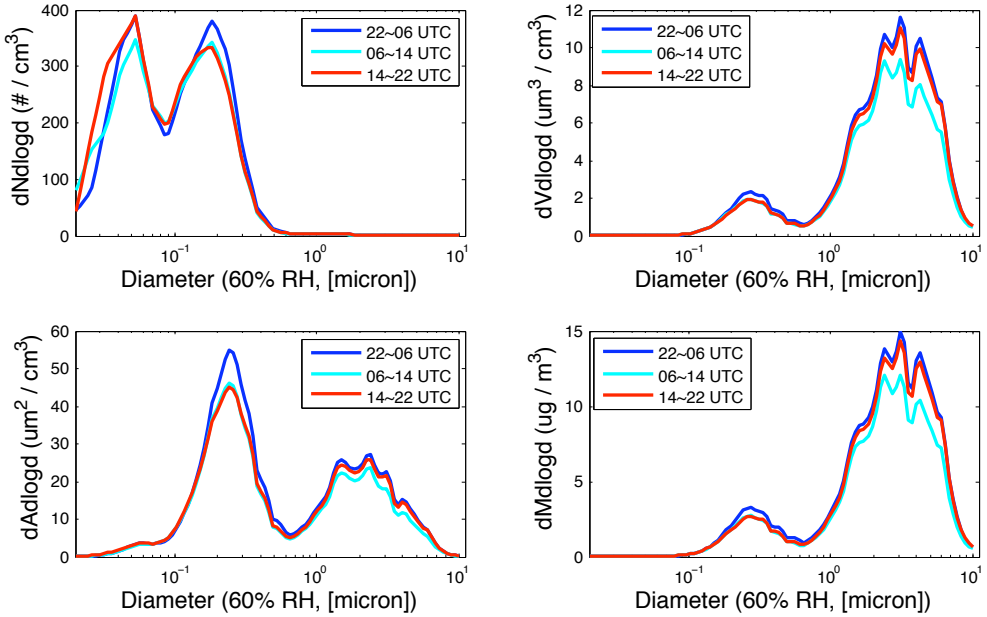

Fig. 8. Mean VOCALS *RHB* particle number (top left), surface area (bottom left), volume (top right), and mass distributions (bottom right) stratified by the time of day in the remote region. The accumulation mode (dominated by SO_4^{2-}) was clearly the largest between near sunset to a few hours before sunrise (22:00 ~ 06:00 UTC), consistent with the observed increase in SO_4^{2-} by the shipboard AMS. More nuclei and coarse mode particles were seen in the afternoon (14:00 ~ 22:00 UTC) than in the early morning (06:00 ~ 14:00 UTC).

ACPD
11, 2873–2929, 2011

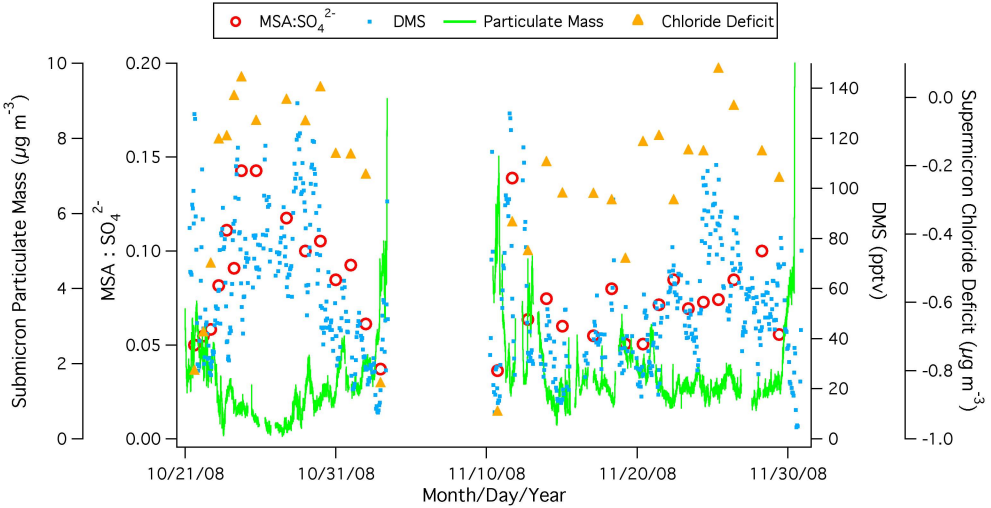

Fig. 9. Time-series of submicron particulate mass, MSA:SO_4^{2-} ratio, DMS, and supermicron chloride deficit. The MSA:SO_4^{2-} ratio follows closely to DMS concentration, while chloride deficit was the largest near the coast, where pollution emission of acidic aerosols were the highest, as evidenced by high submicron mass.

ACPD
11, 2873–2929, 2011

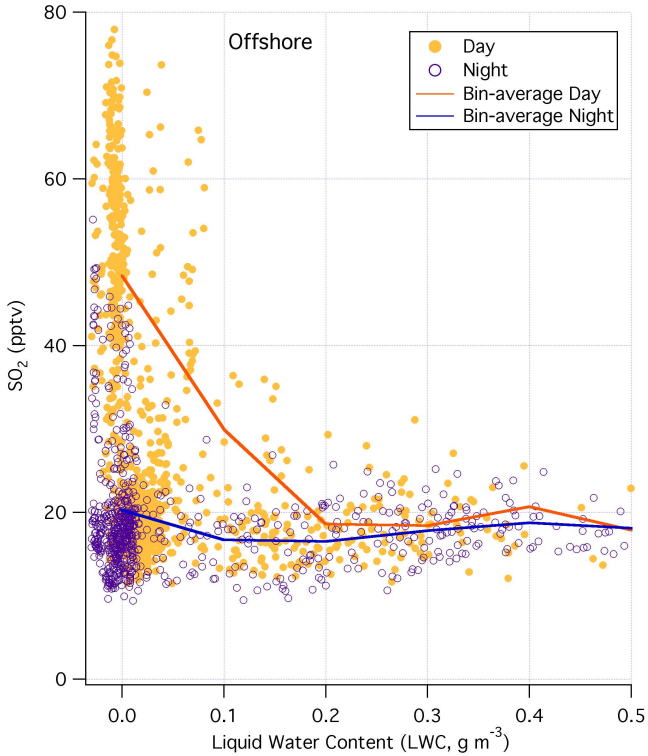

Fig. 10. SO_2 concentration below the inversion vs. liquid water content from the C-130 for the VOCAL offshore region, stratified to daytime and nighttime. Higher SO_2 during the day was due to DMS oxidation. Above 0.2 g m^{-3} (mean L_{WC} for the stratocumulus clouds), SO_2 was reduced to ~18 pptv as a result of in-cloud oxidation. The interstitial SO_2 might be slightly higher during the day due to the initially higher MBL concentration.

ACPD
11, 2873–2929, 2011

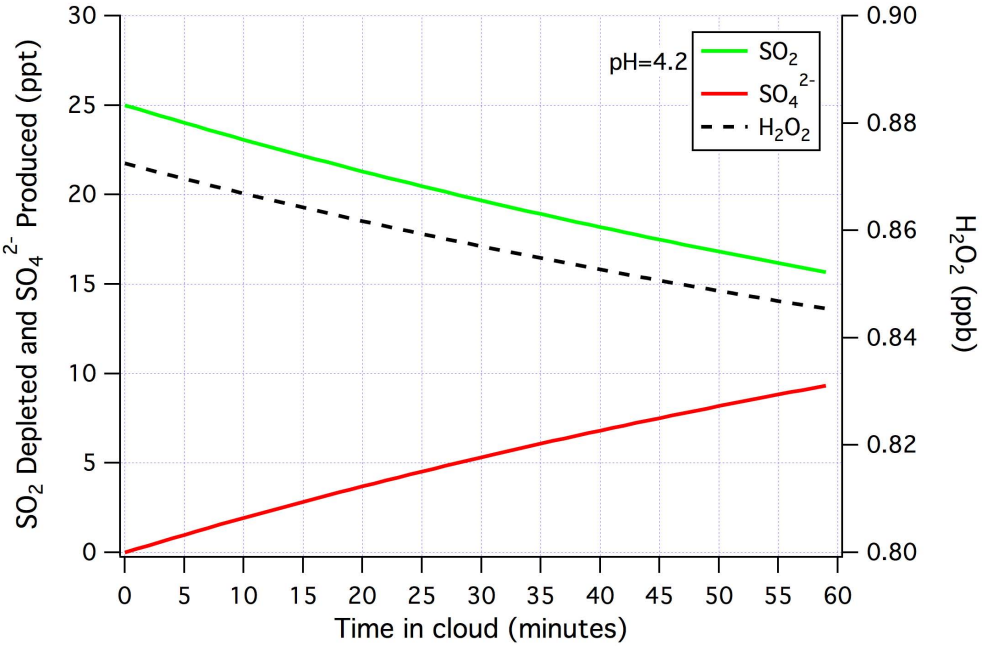

Fig. 11. Calculated oxidation of SO_2 to sulfate in cloud due to H_2O_2 in a closed system. Initial concentrations were set to 20 pptv and 65 µM (~ 0.9 ppb) for SO_2 and H_2O_2. The liquid water content and pH were fixed at 0.2 g m^{-3} and 4.2, respectively. After ~15 min (typical in cloud residence time), 11% of the SO_2 is converted to SO_4^{2-}, leaving an interstitial concentration SO_2 of ~18 pptv.

ACPD
11, 2873–2929, 2011

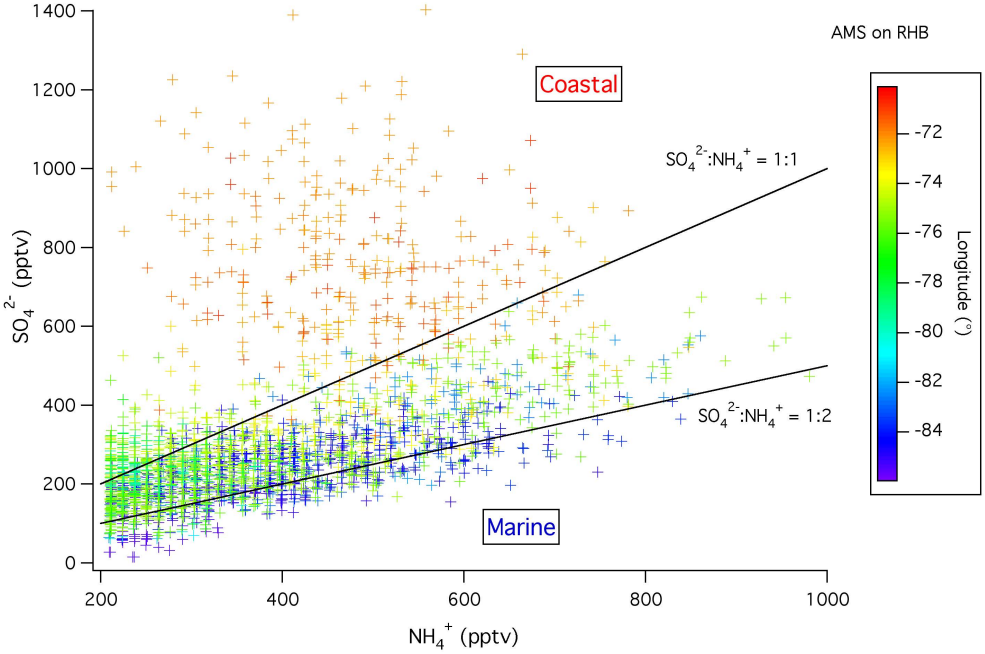

Fig. 12. SO_4^{2-} vs. NH_4^+ from the shipboard AMS, color-coded by longitude. The SO_4^{2-}: NH_4^+ ratio approached the theoretical full neutralization limit of 1:2 for ammonium sulfate in the remote marine region. Closer to shore, the ratio exceeded 1:1 (that of ammonium bisulfate) due to pollution emission.

ACPD
11, 2873–2929, 2011

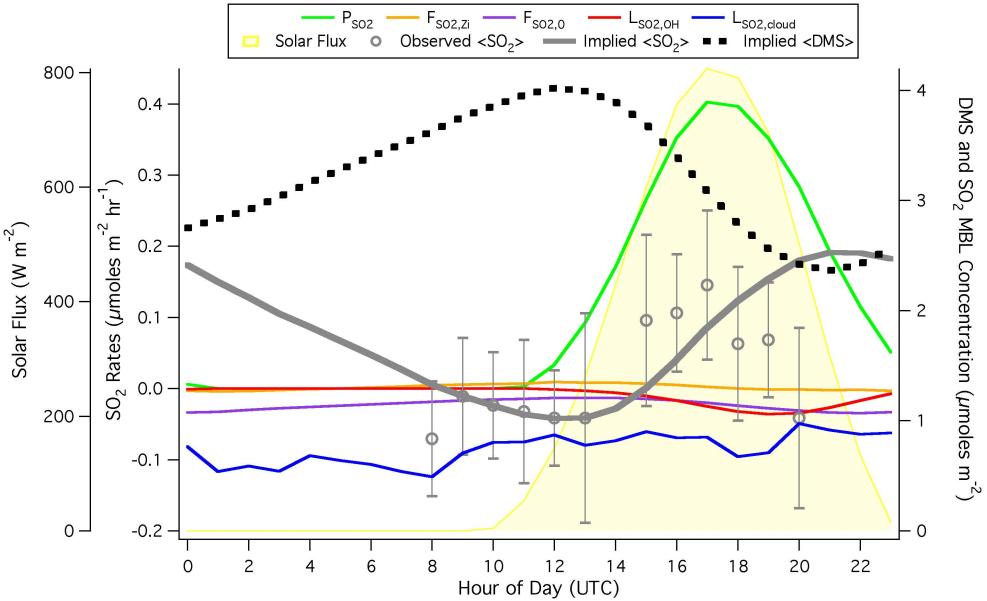

Fig. 13. Implied SO_2 diel cycle, with oxidation from DMS being the principal source and in-cloud oxidation as the main sink. The implied cycle agrees well with observations (gray circles, with error bars corresponding to standard deviation within hour bins) until 15:00 UTC, with measurements in the subsequent hours likely subject to greater spatial bias.

ACPD
11, 2873–2929, 2011

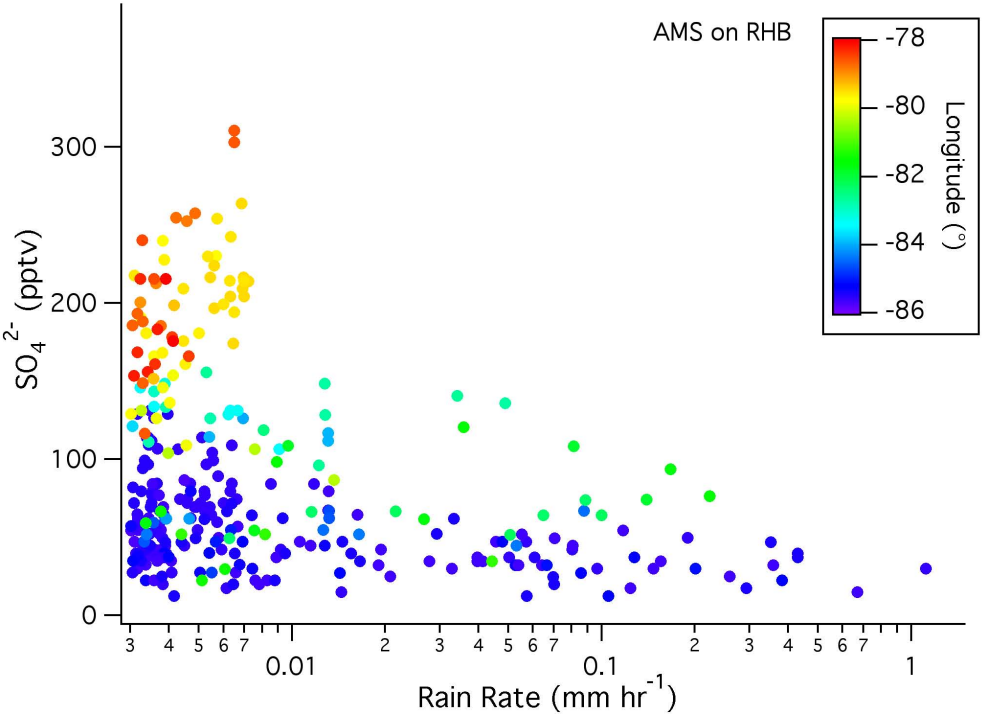

Fig. 14. *RHB* SO_4^{2-} concentration vs. rain rate, color-coded by longitude. While there was clearly a longitudinal trend in SO_4^{2-}, the lowest concentration at 85° W corresponded to high rain rates, suggesting efficient precipitation scavenging.

ACPD
11, 2873–2929, 2011

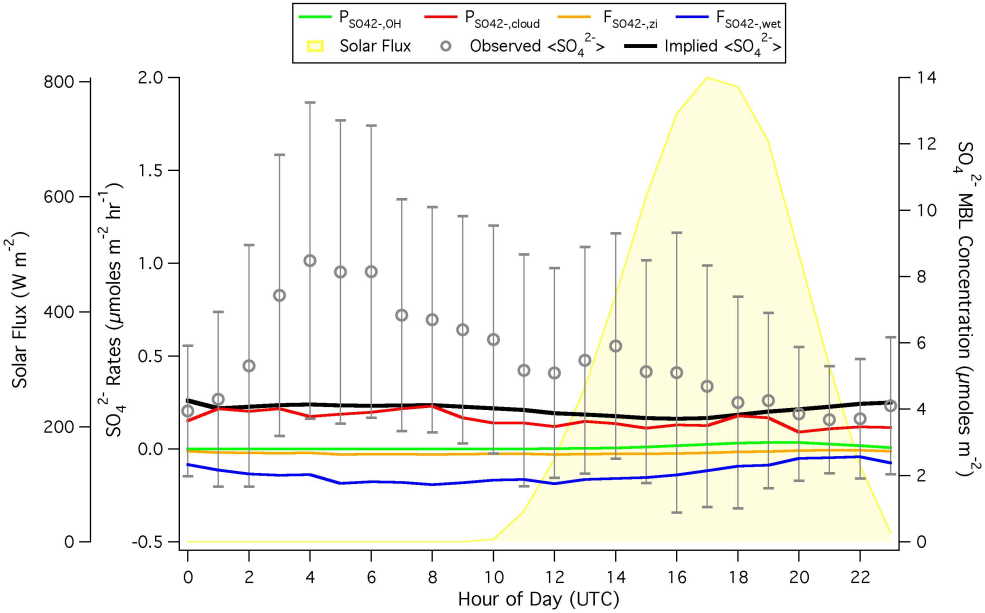

Fig. 15. Implied SO_4^{2-} cycle assuming a well-mixed MBL, with calculation initiated with the observation at 00:00 UTC. The in-cloud production term is largely offset by wet deposition, with gas phase oxidation by OH accounting for the small increase in SO_4^{2-} towards the end of the day. While the source and sink terms appear to balance, the observed diel cycle in SO_4^{2-} (gray circles, with error bars corresponding to standard deviation within hour bins) is not captured by this calculation.

ACPD
11, 2873–2929, 2011

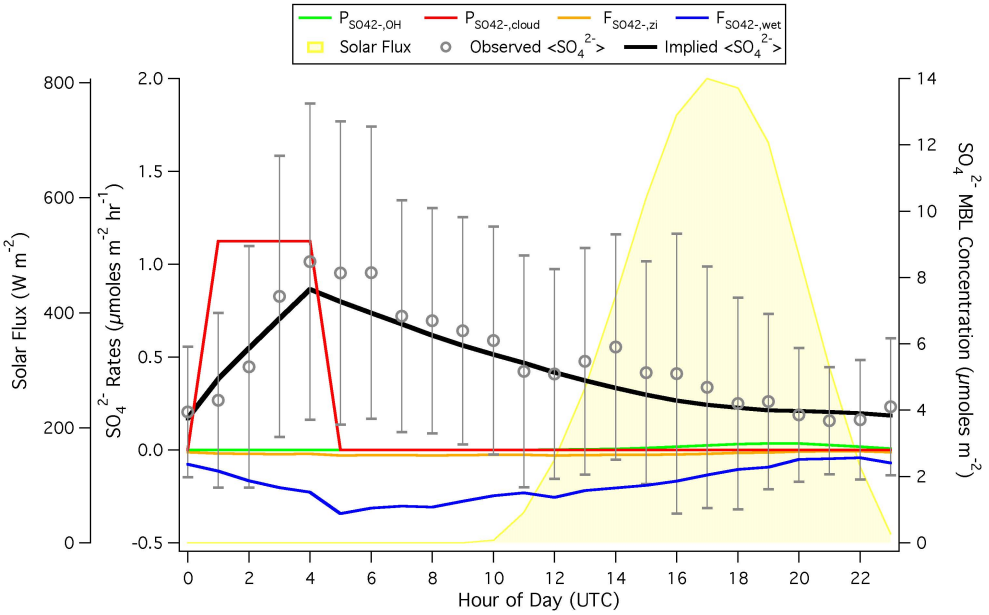

Fig. 16. Implied SO_4^{2-} cycle assuming a well-mixed MBL at night and decoupled MBL during the day. SO_4^{2-} produced in-cloud is summed over the entire day and only added to the MBL budget over the first four hours after sunset as the MBL re-coupled. Initiated with the observation at 00:00 UTC, the implied cycle qualitatively agrees with shipboard observations (gray circles, with error bars corresponding to standard deviation within hour bins).

ACPD
11, 2873–2929, 2011